27 37

LBL-15267
c.2

Lawrence Berkeley Laboratory
UNIVERSITY OF CALIFORNIA

LAWRENCE
BERKELEY LABORATORY
JAN 31 1983
LIBRARY AND
DOCUMENTS SECTION

Invited paper to be presented at NATO Advanced Study Institute, Pearson College, Vancouver Island, B.C., August 23-September 3, 1982; and to be published in the Plenum Press Proceedings

ANOMALONS, HONEY, AND GLUE IN NUCLEAR COLLISIONS

M. Gyulassy

December 1982

NUCLEAR SCIENCE DIVISION

LBL-15267
c.2

Prepared for the U.S. Department of Energy under Contract DE-AC03-76SF00098

DISCLAIMER

This document was prepared as an account of work sponsored by the United States Government. While this document is believed to contain correct information, neither the United States Government nor any agency thereof, nor the Regents of the University of California, nor any of their employees, makes any warranty, express or implied, or assumes any legal responsibility for the accuracy, completeness, or usefulness of any information, apparatus, product, or process disclosed, or represents that its use would not infringe privately owned rights. Reference herein to any specific commercial product, process, or service by its trade name, trademark, manufacturer, or otherwise, does not necessarily constitute or imply its endorsement, recommendation, or favoring by the United States Government or any agency thereof, or the Regents of the University of California. The views and opinions of authors expressed herein do not necessarily state or reflect those of the United States Government or any agency thereof or the Regents of the University of California.

LBL-15267

Anomalons, Honey, and Glue in Nuclear Collisions

M. Gyulassy

Nuclear Science Division
Lawrence Berkeley Laboratory
University of California
Berkeley, CA 94720

ABSTRACT

In these lectures, selected topics in nuclear collisions in the energy range 10^{-1} to 10^{3} GeV per nucleon are discussed. The evidence for anomalous projectile fragments with short mean free paths is presented. Theoretical speculations on novel topological nuclear excitation and on quark-nuclear complexes in connection with anomalons are discussed. Recent tests for pion field instabilities are presented. Then evidence for collective nuclear flow phenomena are reviewed. Global event analysis and cascade simulations are presented. We address the question of whether nuclear flow is like viscous honey. Finally, the criteria for the production of a quark-gluon plasma are discussed. Nuclear stopping power and longitudinal growth at high energies are considered. Results from cosmic ray data show that nuclear collision at TeV per nucleon energies are likely to produce a plasma.

1. INTRODUCTION

In these lectures, I will cover three rapidly evolving areas of current research in the field of high energy nuclear collisions. Extensive reviews of additional topics can be found in Refs. (1,2). The topics covered here address the following questions:

1) Do novel nuclear states exist?

2) Do nuclei flow like honey?

3) Can a quark-gluon plasma be produced?

These questions span a wide energy range from ~200 AMeV (topic 2), ~2 AGeV (topic 1), to ~1 ATeV (topic 3). (Note AMeV ≡ MeV per incident projectile nucleon, etc.) In section 2, I discuss the evidence for anomalons. These are relativistic nuclear fragments that tend to interact much more frequently in matter than do familiar nuclei with the same charge. Various speculations about these objects are discussed. In particular, we ask whether anomalons could be hungry quark with a ravenous appetite for nucleons. I also discuss the status of the search for pion field coherence in nuclear collisions. With regard to question 2, I review in Section 3 the in(con)clusive data showing that collective nuclear flow could take place at lower energies. This question is of interest because through the flow characteristics we hope to learn about the nuclear equation of state at high densities. Then the topic of global event analysis is discussed and cascade calculations illustrating various flow phenomena and presented. Finally, in Section 4, boosting ourselves to the erg per nucleon (ATeV) energy region, the prospects of probing the quark-gluon plasma are analyzed. Nuclear stopping power and longitudinal growth are discussed. Cosmic ray data with events showing charge particle multiplicities

up to 1000 are analyzed. These data are interpreted as showing that high enough energy densities can indeed be achieved in nuclear collisions to produce an ideal quark-gluon plasma.

2. NOVEL NUCLEAR STATES

2.1 Anomalons

Since early cosmic ray studies, there have been recurring observations in emulsions of anomalous projectile fragments.[3-6] These fragments are anomalous because their reaction mean free path, $\lambda_a(Z)$, is much smaller than expected for nuclei with charge Z. Primary nuclei with $2 \leq Z \leq 26$ and kinetic energy between 0.2 and 2.0 AGeV are found to have a mean free path

$$\lambda(Z) = \left\{ \sum_{A \epsilon Em} \rho_A \, \sigma_A(Z) \right\}^{-1} \quad , \tag{2.1}$$

where ρ_A is the density of nuclei with atomic number A in emulsions and $\sigma_A(Z)$ is the usual geometrical cross section ($r_o \approx 1.2$ fm)

$$\sigma_A(Z) \approx \pi r_o^{\,2} \, (A^{1/3} + (2Z)^{1/3})^2 \quad . \tag{2.2}$$

Eqs. (2.1, 2.2) arise because normal nuclei behave essentially as black discs. Often it is convenient to group all charges together by parameterizing

$$\lambda(Z) = \Lambda^* Z^{-b} \tag{2.3}$$

Measurements of primary mean free paths[5,6] give $\Lambda^* \approx 25$–30 cm and $b \approx 0.34 \pm 0.3$.

In practice Λ^* is determined by measuring path lengths l_i traversed by many nuclei and counting the total number of interactions according to

$$\Lambda^* = \sum_{D<l_i<D+\Delta} (l_i - D) \, Z_i^b / N(D,\Delta) \quad , \tag{2.4}$$

where D is an arbitrary distance into the emulsion and $N(D,\Delta)$ is the number of interaction stars observed between D and $D+\Delta$. By the definition of mean free paths, Λ^* should be independent of both D and Δ. As shown in Fig. 1, such an independence of Λ^* on D and Δ is indeed observed[6] for primary nuclei (in this case, O^{16}).

However, the mean free paths of secondary fragments produced in nuclear collisions at ~2 AGeV do appear to dependent on D. A "typical" multichain event seen in the emulsion is shown in Fig. 2. An incident ^{56}Fe beam collides with an Ag or Br nucleus producing among other fragments a charge Z=9 relativistic fragment. At a distance X from the primary vertex that relativistic fragment collides with another emulsion nucleus. A tertiary fragment with Z=8 is produced. This propagates a distance Y before it too interacts in the emulsion. For this event $l_i = X$ and D is the distance from the primary vertex when used in Eq. (2.4). On the order of 1000 events with secondary interactions have been analyzed in this way.

In Fig. 3 we see the striking result of that analysis. While $\Lambda^*(D)$ is independent of D for distances $D > 5$ cm from the primary vertex, there appears to be a significant reduction of Λ^* for $D < 5$ cm (Δ is typically ~1 cm in this analysis).

As a parametrization to account for this dependence on D, the following model was proposed in Refs. (3,6): They assumed that a fraction α of all secondary fragments have an anomalously short mean free path λ_a. The solid curve in Fig. 3 was obtained by setting $\alpha = 0.06$ and $\lambda_a = 2.5$ cm. In Fig. 4 the likelihood function for different values of α and λ_a is shown. The greatest compatibility with the data is achieved for $\alpha < .2$ and $\lambda_a < 6$ cm. For comparison, primary nuclei with $Z < 26$ have $\lambda(Z) \gtrsim 10$ cm. Of course this

parametrization is not unique. In Ref. (5) an equally good fit was obtained by assuming that 100 percent of the secondaries are anomalous but that this anomalous property decays away after $\sim 10^{-10}$ sec.

A rather mysterious property of anomalons is that global reaction characteristics, e.g., the heavy prong-multiplicity distribution $P(N_h)$, of anomalous and normal nuclear reactions do not seem to differ. In addition, there is (weak) evidence[6] that anomalons tends to produce anomalons. Thus in Fig. 2, if X is short compared to $\lambda(Z)$, then Y is also likely to be short compared to $\lambda(Z)$. This has been called the memory effect. Finally, the anomalous effect is seen convincingly only for fragments with $Z \geq 3$.

These observations taken together rule out many conventional explanations. For example, they cannot be hyper fragments or pionic atoms because the decay of these secondaries would result in the enhancement of $P(N_h)$ for $N_h = 0,1$. Such enhancement is ruled out by the data. Nuclear molecules[7] cannot account for the observation of anomalons with $Z < 10$ nor the apparent memory effect. Neutron excess isotopes[7] cannot account for the dependence of Λ^* on D. Finally, ordinary nuclear excitations have too short a lifetime $\ll 10^{-10}$ to account for these results.

We are thus left with a puzzle. However, it is important to emphasize that only limited statistics are available and unknown systematic biases may plague emulsion data. Much higher statistics and different techniques will be needed before these anomalons can be regarded as proven. Today we can only say that this observation is the most baffling result obtained thus far at the Bevalac.

2.2. Hungry Quarks

Because anomalons are so weird, they have fueled theoretical speculations beyond the conventional boundaries of nuclear physics. Probably all such

speculations are wrong, but they illustrate well how little we really know about nuclear or hadronic matter under extreme conditions of high density and temperature. In this section, I expose two wild speculations: topolons and hungry quarks.

Topolons is a generic name I give to novel topological configurations of hadronic matter. Since Wheeler, many calculations have exploited topological degrees of freedom. The main problem that cast doubt on past calculations was the stability of such configuration. More recently, it has been realized that certain classes of field theories possess nontrivial topological sectors with conserved topological quantum numbers. In particular, effective chiral Lagrangians exhibit this phenomenon.[8] Thus, the problem of stability is solved by a new conserved quantum number. These topological excitations possess rather shocking properties such as an effective fractional charge. In the model proposed in Ref. (8), the solitons predicted have the additional weird property of having high baryon <u>and</u> strangeness (>6 in magnitude). Since these states correspond to large extended objects, production of them in e^+e^- or pp collisions is suppressed by form factor and tunneling effects. However, in nuclear collisions extended objects are easy to create and a baryon number reservoir is readily available. Multiple strangness can also be produced (more easily) through the many independent NN collisions. It is thus remotely possible that anomalons are topolons.

Further support of this conjecture can be found in the work of Boguta[9] who was able to construct chiral models consistent with normal nuclear properties. Obviously any model proporting to predict a new state of matter must be compatible with the old well loved ones. By introducing an effective gauge theory for nuclear matter, Boguta finds that not only can normal finite

nuclear properties be accounted for but also new topological excitations can be found. He calls them hadroids. Such calculations are still very preliminary but indicate that anomalons could be made compatible with nuclei within an effective chiral theory of nuclear matter.

Another exotic line of speculation revolves around the heretical view that maybe QCD is not the final word on the subject. Suppose that color is not rigorously confined! It could be that color SU(3) is spontaneously broken by some nasty Higgs mechanism.[10-13] If that is the case, then there could exist colored nuclear states or quark-nuclear complexes.

As a fun example of what such states could look like, I review the hungry quark states suggested in Ref. (10). Suppose that we add an effective interaction $L' = \mu^2/2\, A_{\mu a}A^{\mu a}$ to the QCD Lagrangian. (There is considerable debate on whether such an addition is consistent with verified QCD predictions[11].) Thus, we suppose that gluons have a small mass μ. Consider now an MIT bag in which we place a <u>static</u> color source density ρ_a. The color potential then satisfies:

$$(\nabla^2 - \mu^2)\, A_a^0 = -g\rho_0 \tag{2.5}$$

Integrating eq. (2.5) over the bag volume V and noting the boundary condition $n\cdot\nabla A_a^0 = 0$ on the surface, one finds that

$$A_a^0 = \frac{gQ_a}{\mu^2 V} + O(\mu^0) \tag{2.6}$$

where $Q_a = \int_V \rho_a$ is the total color charge. Thus, there is a field energy

$$E_F = g/2 \int_V A_a^0 \rho_a \approx \frac{2\pi\alpha_s}{\mu^2 V} C^2 \tag{2.7}$$

where $\alpha_s = g^2/4\pi$ and $C^2 = \Sigma Q_a^2$ is the Casimir of SU(3). (C^2 = 16/3, 12 for 3 and 8 representations). Eq. (2.7) shows that if $\mu \longrightarrow 0$ the field energy diverges. Thus, confinement of color arises only if $\mu = 0$. However, for $\mu \neq 0$ the colored state has finite energy $E = E_F + BV$, where $B \approx m_\pi^4$ is the vacuum pressure. Minimizng with respect to V, Ref. 10 finds the mass and radius of the state is

$$M = 2BV \approx 10 \text{ GeV} \left(\frac{18\text{MeV}}{\mu}\right) r^{1/2}$$
$$R = 2.8 \text{ fm} \left(\frac{18 \text{ MeV}}{\mu}\right)^{1/3} r^{1/6} \tag{2.8}$$

where $r = 3C^2/16$. Note r = 1 for a quark like state and r = 9/4 for a gluon like state.

Thus, in this model a bare quark weighs ~10 GeV and has a radius ~3 fm. The reason it is so big is that the enormous color field pressure inside can push back the vacuum pressure B confining the quark to the bag. As shown in Ref. 10, such quark states are unlikely to have been produced in e^+e^- or hh collisions due to a large form factor suppression.

The most interesting property of these quark states is their appetite for nucleons. This is estimated by assuming that a nucleon unfortunate enough to get inside a quark bag will be dissolved into its constituents. (By definition the inside of a bag corresponds to the perturbative phase.) Adding A nucleons, a Fermi sea of up-down quarks is thereby filled up in the bag to a Fermi momentum k_F:$(2k_F^3/\pi^2 = 3A/V)$. The energy of this sea is

$$E_{sea} = V \frac{3\ k_F^4}{2\pi^2} f \tag{2.9}$$

where f is a fudge factor incorporating interactions in the sea: $f = 1 + 8\alpha_s/3\pi \approx 1.5$ for the MIT bag. Minimizing the total energy $E_F + BV + E_{sea}$ with respect to V gives

$$M = M_Q \frac{1 + x}{\sqrt{1-x}}$$

$$V = \frac{M_Q}{2B} \frac{1}{\sqrt{1-x}}$$

$$A = \frac{M_Q}{3\sqrt{\pi}B^{1/4}} \frac{(2x/f)^{3/4}}{\sqrt{1-x}} \quad , \qquad (2.10)$$

where $x = E_{sea}/3BV$ is the ratio of the pressure exerted by the sea to that of the vacuum. M_Q is given by eq. (2.8). Quarks will continue to eat nucleons as long as

$$\mu = \frac{\partial M}{\partial A} = 3\ (2\pi^2 Bx)^{1/4}\ f^{3/4} \leq M_N \qquad (2.11)$$

The value of A for which $\mu = M_N$ gives the appetite of the quark. Give the volume V, the mean free path $\lambda_Q(A)$ of this object in emulsion is given by Eq. (2.1) with $\sigma_A(Z)$ replaced by

$$\sigma_{AQ} \approx \pi \left(r_o A^{1/3} + (3V/4\pi)^{1/3}\right)^2 \qquad (2.12)$$

In Fig. 5, the ratio of $\lambda_Q(A)$ to $\lambda(A)$ for normal nuclei with atomic number A and the energy per nucleon M_Q/A of the fat quark are shown versus A. We see that for "reasonable" fudge factors $f \sim 1.5$, up to 20 nucleons can be eaten by a quark. The weight of this satiated quark is ~2 GeV per nucleon. By fudging a little ($f \sim 1.2$) this mass can be brought down but then λ_Q/λ_A is no longer less than 1. In fact, such quark-nuclear complexes may be even <u>smaller</u> than normal nuclei.

This fun calculation illustrates that if QCD is slightly broken, then rather weird and perhaps anomalous phenomena could arise in nuclear collisions. Therefore, it is worthwhile to keep an eye out for such beasts.

The predicton of this model that is easiest to test is the occurrance of fractionally charged, high baryon number fragments. Currently, plastics give the highest charge resolution and experiments by the Price group[14] are being carried out. The preliminary results indicate no fractionally charged nuclei observed at a level of 10^{-3}. If this result is confirmed, then a large class of speculations can be ruled out at this energy range. Of course, integral charged topolons and glue-nuclear complexes could still be responsible for anomalons in that case.

A natural question at this point is why we have not observed any of these novel objects in e^+e^- or pp collisions. In order to produce colored states it is necessary to pull two quarks or gluons apart by at least $2R_Q$, where $R_Q \sim 3$fm is the radius of the quark bag. However, as we try to pull a quark and antiquarks apart, a color electric tube of area $a \simeq 4\alpha_s\pi^2\alpha'$ and electric field $E = g/a$ is formed. Numerical estimates give $gE \sim 1.8$ GeV/fm. Using the Schwinger formula[15] the probability that no quark-antiquark pairs are produced by that electric field in a tube of length $2R_Q$ is given by

$$P_o(2R_Q) \sim \exp\left[-\frac{2}{3}\alpha_s gER_Q^2\right] \sim \exp\left[-3(R_Q/\text{fm})^2\right] \qquad (2.13)$$

If $R \sim 3$fm, then there is only a 10^{-12} probability that the tube can be stretched out far enough without creating additional pairs that neutralize the color field. It is thus far more likely that several pairs are produced in the flux tube before the tube reaches the critical size ~6 fm necessary to isolate

quarks. The advantage offered by nuclei is that they are big. If a quark-gluon plasma can be produced in nuclear collisions (see Sec. 4), then a quark and antiquark can separate by twice the nuclear radius without forming a flux tube. That is because the plasma state is perturbative. Once having separated by that large distance a rearrangement of field configurations could then lead to the production of isolated extended quarks.

Finally, we note that cosmological evidence for the existence or non-existence of such objects is extremely ambiguous. For example, Ref. (16) showed that, under a variety of plausible scenarios, the number of relic diquarks per nucleon lies somewhere within the narrow range 10^{-50} to 10^{10}! Clearly, the door is open to discovery. Nuclear collisions may hold the key to that door.

2.3 Last Bastion of Pion Condensation

The last topic on novel nuclear excitations that I cover here is pion field instabilities. In the past decade much interest has focused on possible pion field instabilities in nuclear matter at high densities.[17] Nuclear collisions at several hundred MeV per nucleon were recognized[18] as one of attractive ways to search for such phenomena. Simple estimates showed that densities up to $\rho \sim 4\rho_0$ ($\rho_0 = 0.145\ \mathrm{fm}^{-3}$) could be easily generated. However, along with high densities high internal excitation energies must also be taken into account. In particular, the non-equilibrium configuration of two interpenetrating nuclear fluids should be considered. This configuration is characterized by the momentum space distribution

$$n(p) = \theta(p_F - |\underset{\sim}{p} + \underset{\sim}{p}^*|) + \theta(p_F - |\underset{\sim}{p} - \underset{\sim}{p}^*|) \ . \qquad (2.14)$$

We consider whether there are pion field instabilities in such a configuration. This problem is then analogous to the study of the two-stream instability in colliding plasmas.

The starting point is the calculation[18] of the pion propagator in nuclear matter with a momentum distribution given by Eq. 2.14. The essential point is that the pion self energy for $\omega = 0$ modes is controlled by the particle hole propagator, $\pi_0(\omega,k)$, which is the Lindhard function appropriate for a zero temperature Fermi gas with Fermi momentum p_F. Recall[18] that for $\omega = 0$, Re $\pi_0(0,k) \propto p_F$ and that π_0 is proportional to the pion self energy in one isolated Fermi sphere. With eq. 2.14, each Fermi sphere is boosted and therefore the self energy is Doppler shifted[18]

$$\pi(\omega,\underset{\sim}{k}) = \pi_0(\omega+\underset{\sim}{v}^* \underset{\sim}{k},\underset{\sim}{k}) + \pi_0(\omega-\underset{\sim}{v}^*\cdot\underset{\sim}{k},\underset{\sim}{k}) \tag{2.15}$$

Eq. (2.15) shows that the only standing waves ($\omega = 0$) in the non-equilibrium configuration that remain standing waves in the isolated Fermi spheres are those with $\underset{\sim}{v}^* \cdot \underset{\sim}{k}=0$. In other words, only pion wave vectors $\underset{\sim}{k}$ that are perpendicular to the beam axis can remain standing in the non-equilibrium configuration. Furthermore, for such perpendicular modes there is a large <u>dynamical</u> enhancement of the self energy

$$\pi(0,k_\perp) = 2\,\pi_0(0,k_\perp) \approx \pi_0(0,k_\perp)\,|_{\rho=8\rho_0} \tag{2.16}$$

Indeed, detailed calculations[18] showed that pionic instabilities are concentrated in modes perpendicular to the beam axis. The growth rate of those

modes were found to be $\gamma(k) \sim 0.1m_\pi$ for $k_\perp \sim 2m_\pi$. The large magnitude of the wave vector follows from the p-waves nature of the πNN interaction.

How would one look for such an instability? The main effect of such an instability would be the growth of a collective spin-isospin wave in the medium.[19] Because the spin-isospin current is a source of pions, any time dependent spin-isospin wave would radiate pions. In particular, the invariant inclusive pion distribution is given by

$$\omega_k \frac{d^3n}{dk^3} = \frac{1}{2(2\pi)^3} \int d^4x d^4y \; e^{-ik(x-y)} \langle in | j_H^+(x) j_H(y) | in \rangle \qquad (2.17)$$

where $|in\rangle$ is the state of two colliding nuclei and $j(x)$ is the divergence of the axial vector current. Thus, the pion spectra measure the on-shell Fourier transform of the spin-isospin current fluctuation. If a macroscopic collective current is generated through an instability, then eq. (2.17) reduces to the well-known formula for radiation

$$\omega_k \frac{d^3n}{dk^2} = \frac{1}{2(2\pi)^3} \; |j(\omega_k, k)|^2 \qquad (2.18)$$

Based on the growth rates computed in Ref. 18 and the mean field results for $j(x)$ in the presence of a pion condensate,[20] a model for the transient growth of $j(x,t)$ was constructed in Ref. 19. The predicted pion spectra are shown in Fig 6. Although the magnitude of the pion radiation is very small, the predicted peaking of the coherent yield at large perpendicular momenta ($k_\perp \sim 2m_\pi$) makes it possible to search for this tiny signal amidst the incoherent pion yield. At high energies ($\geq$400 MeV/nucleon), ordinary incoherent NN$\rightarrow$NNπ processes dominate. However, below threshold the incoherent

pion component is greatly suppressed, while the coherent pions due to pionic instabilities are approximately beam energy independent. This is because for perpendicular modes the self energy, eq. (2.15) is independent of p*.

New data[21] at 0.2 GeV/nucleon have provided a stringent test for coherent pions generated via pionic instabilities. As seen from Fig. 6, the incoherent background is suppressed a factor 10^5 relative to the 2 GeV/N yield at $k_\perp \sim 2m_\pi$. Unfortunately, no deviation from a pure (phase space) exponential is observed. Therefore, these data rule out the possibility of a collective spin-isospin wave in this reaction.

At least two possible explanations for the results in Fig. 6 can be put forward. First, if the effective Migdal parameter g',[17] representing all other interactions in the pion channel besides one pion exchange is large (g'>0.6), then no instability can occur.[18] Second, Ne may be too small a system and too diffuse to be able to support a spin-isospin wave of wavelength $\lambda = 2\pi/k \sim 4.4$ fm. The second possibility is being tested currently via a similar experiment involving Xe+Xe. However, other searchers[22] for critical pion field effects tend to support the first explanation. In any case, Fig. 6 is an impressive demonstration of the high sensitivity achieved in present experiments, which now explore cross sections down to $1\mu b/GeV^2$ and have the ability to search for such needles in a haystack. If no positive results are observed with Xe + Xe, the last bastion of pion condensation will shift to the cores of neutron stars.[23]

3. DO NUCLEI FLOW?

3.1 In(con)clusive Data

One of the main goals[1,2] of studying nuclear collisions is to extract some information on the nuclear matter equation of state at high densities and

temperatures. However, this program has turned out to much more difficult than first hoped. The main reason is that the reaction mechanism is very complex with many competing processes going on simultaneously. In typical inclusive data we see the convolution of geometrical effects (impact parameter), finite mean free path effects (non-equilibrium phenomena), initial state interactions (Fermi motion, clusterization), and final state interactions (Coulomb and coalescence) in addition to whatever equilibrium and collective phenomena that may have occurred.

Figure 7 illustrates the dilema. In Fig. 7 A hydrodynamic calculations[24] are compared with the double differential charge inclusive ($\sigma_p + \sigma_d + 2\sigma_\alpha + \ldots$) data of Ref. (25). In Fig. 7 B cascade[26] calculations are compared to the same data. Although the dynamical assumptions of the two calculations contradict each other (hydrodynamics assumes zero mean free path while cascade assumes long mean free paths), they both reproduce the inclusive data to the same accuracy. We now understand this to be a simple reflection of the fact that geometry and phase space control inclusive cross sections.[1]

In order to gain sensitivity to the dynamics, more exclusive data need to be analyzed. In Fig. 8, data on centrally triggered (high multiplicity) events are shown. By selecting a high multiplicity, the trivial convolution of impact parameters is reduced, the non equilibrium component is minimized, and the probability of finding signatures of bulk equilibrium dynamics is maximized. The first feature to observe is that by triggering on small impact parameters, the theoretical predictions[27] of cascade and hydrodynamical models differ substantially. Cascade models predict that the inclusive yields are maximum at forward angles, while hydrodynamic models predict a sidewards emission of particles. These calcuations refer to the matter flow including

p, d, t, α, ... The proton data[28] are shown in the middle left. The great excitement arose initially because it seemed that for the first time hydrodynamic calculations were closer to the observed angular distribution than were cascade predictions. Since then the size of the experimental error bars were found to be too optimistic. Preliminary high statistics plastic ball results[29] show only a flattening at forward angles with no dip at 0°. In addition, preliminary neutron spectra[30] have caused havoc by showing a large forward enhancement in accord with cascade results. It was also realized[31] that copious production of composite fragments in the forward direction could cause a depletion of the unbound proton yield at zero degrees. Thus, Fig. 8 can no longer be regarded as evidence for hydrodynamical flow.

Another observation which suggested nuclear flow phenomena is the difference between the "temperature" (slope parameter of the inclusive 90° cm yield) of protons and pions.[32] The idea was that a radial exploding fireball naturally leads to a difference on the slope parameter due to simple kinematics of superimposing collective and random motions for different mass particles. However, the recent observation[1] of an apparent kaon temperature exceeding that of protons contradicts such a model unless kaons are assumed to be decoupled from the flow. Hence, this evidence is also inconclusive.

The most recent attempt to find evidence for compression effects was reported in Ref. (33). An outstanding problem in this field is to understand the excitation function of pions, i.e., the magnitude and dependence of the average number of pions produced versus beam energy. In Fig. 9, the measured data are compared to Cugnon cascade[26] calculations. This cascade code reproduces correctly the pion yield in proton induced reactions yet is seen to

over predict it for nuclear reactions. One of the obvious potential deficiencies of the cascade code has been ruled out. Namely, it could be that pion absorbtion is much stronger in dense nuclear matter than ordinary nuclear matter. However, cascade predicts that at higher energies, higher densities $\rho \sim 4\rho_0$ are achieved. Therfore, if the discrepancy were due to a poor pion absorbtion mechanism, then the discrepancy should be largest at the high energy region. The contrary is observed. Why then does cascade predict too many pions?

The suggestion in Ref. (33) is that due to nuclear repulsion at high densities, not as much energy is available for the production of pions as there would be if there were no potential energy. Indeed one of the main effects neglected in cascade calculations is the nuclear mean field. By assuming that the discrepancy in Fig. 9a is due solely to the neglected potential energy, the potential energy curve for densities up to $4\rho_0$ was obtained as shown in Fig. 9b. This remarkable curve is the first tentative extraction of the nuclear equation of state using nuclear collision data! As such it is a landmark in this field. Note that a very sensible equation of state with compressibility $K \sim 250$ MeV is found.

However, this interpretation of the pion discrepancy is still under debate and many questions need to be answered before Fig. 9b can be accepted. The Cugnon cascade code does a rather good job in accounting for the inclusive charge sum and primordial deuteron spectra (see Fig. 7 B). Would these predictions be changed for the worse by including potential effects? If the cascade code is altered to account for the pion yield, what other observables are changed? Also it is known that hydrodynamical calculations of the pion multiplicity <u>underestimate</u> the pion yield by a factor of ~1/2. However, such

calculations include via an assumed equation of state the compression energy. Furthermore, the pion yield is found to be insensitive[34,35] to the compressibility constant, K, assumed. This insensitivity follows because most of the entropy is produced via shock waves. However, baryon and four momentum flux conservation (Rankine-Hugoniot equation) severely limits the magnitude of the pressure and entropy that can be achieved in shocked matter.[35] Figure 10 illustrates the problem. The dynamical path (density and temperature versus time) followed in a collision does in fact depend on the equation of state. For a compression energy rising linearly with density (ρ) an 800 meV/nucleon collision reaches a maximum $\rho \sim 4\rho_0$ and $T \sim 140$ MeV. Subsequent isentropic expansion is indicated by the shaded area. On the other hand, for a compression energy rising quadratically (ρ^2) only $\rho \sim 3\rho_0$ is reached with $T \sim 110$ MeV. Now comes the catch. The isentropic expansion from the maximum compression point leads to nearly the same freezeout temperature $T_f \sim 60$ MeV at $\rho_f \sim \rho_0$. Since $\langle N_\pi \rangle$ is uniquely determined by T_f and ρ_f, we conclude that $\langle N_\pi \rangle$ is insensitive to the equation of state if pions are in chemical equilibrium.

However, $\langle N_\pi \rangle$ is rather sensitive to viscosity effects.[34] Figure 11 shows the same data as in Fig. 9 together with ideal hydrodynamic ($\eta = 1$) predictions. By allowing for a 20 percent increase of the entropy due to viscous heating (curve $\eta = 1.2$) rather satisfactory agreement can be found between data and calculation. Notice that a simple fireball model (FB) overestimates the pion yield even more than cascade. Therefore, compression effects are indeed important in reducing the entropy. However, Fig. 11 shows that viscocity effects may be crucial in getting $\langle N_\pi \rangle$ right.

We conclude that while Fig. 9 is provocative, alternate explanations of the data that are not sensitive to the compression energy can also be advanced at present. This debate is far from settled, and it will take some time for the dust to settle.

3.2 Global Analysis

A powerful new method has been developed recently to search for compression effects directly. This involves looking for collective flow patterns on an event by event basis. Such global analysis requires the measurement of as many fragments as possible per event. The elaborate detector[38] called the Plastic Ball/Wall is now in operation and has the capability of measuring the mass m_ν and momenta $\underset{\sim}{p}(\nu)$ of several hundred charged particles at once. In addition, streamer chamber photographs[39] provide a means to measure the momenta of all charged particles on an event by event basis. How can we best extract flow information from such charge exclusive data?

In high energy physics several global variables have been defined that have great intuitive appeal. These include the well known thrust and sphericity variables

$$T = \max_{\hat{n}} \sum_\nu |\underset{\sim}{p}(\nu)\cdot\hat{n}| / \sum_\nu |\underset{\sim}{p}(\nu)| \quad , \tag{3.1}$$

$$S_{ij} = \sum_\nu p_i(\nu) p_j(\nu) \quad , \tag{3.2}$$

The sphericity tensor provides the simplest three dimensional event shape parametrization. However, for nuclear collisions it is necessary to modify S_{ij} in order to take into account the copious production of nuclear fragments with $A > 1$. This is necessary because we do not want to weigh the contribution from an α particle more than four unbound collinear nucleons in determining the flow pattern.

One way to achieve the correct weight is to calculate the kinetic flow tensor

$$F_{ij} = \sum_{\nu} p_i(\nu) p_j(\nu)/2m_\nu \tag{3.3}$$

Other weights,[37] eq. $|\underset{\sim}{p}(\nu)|^{-1}$, can also be used. F has the advantage that for energies $\lesssim 1$ AGev, TrF is the observed kinetic energy in the cm frame. (Of course, global analysis must be performed in the nucleus-nucleus center of mass). Since F is a symmetric matrix, it is readily diagonalized

$$F = \sum_{i=1}^{3} f_i e_i e_i^{+} \quad , \tag{3.4}$$

where f_i are the flow eigenvalues and e_i are the orthonormal engenvectors specifying the principal axes. Therefore, F characterizes an event as an oriented ellipsoid with radii $\sqrt{f_i}$ in momentum space. The angle θ_F between the principal axis carrying the maximum kinetic energy and the beam direction is called the flow angle.

In order to display the flow characteristics we proposed the following flow diagram:[36] Plot θ_F versus the kinetic flow ratio $r = f_{max}/f_{min}$. In momentum space $\sqrt{r}$ gives the aspect ratio of the ellipse in the plane of the major and minor axis of the event. The insert in Fig. 12 illustrates how an actual measured event (400 AMeV Ca + Ca) recorded by the Plastic Ball is represented by this flow analysis. That event corresponds to $\theta_F \simeq 19°$ and $r = 3$.

Also shown in Fig. 12 are the results of calculations[36] using the Cuguon cascade and hydrodynamics for the reaction $^{238}U + ^{238}U$ at 400 AMeV. It is immediately obvious that there is substantial difference between the flow

characteristics expected with non-viscous hydrodynamics and that expected with cascade. For such heavy systems finite number fluctuations are not important. However, as shown in Ref. (36) for systems involving nuclei with $A < 100$, finite number effects lead to very large fluctuations and tend to obscure the picture. Fortunately, with the new Uranium capability of the Bevalac, experiments with heavy nuclei have become possible.

Non-viscous hydrodynamics predicts much stronger sidewards flow than cascade does. Cascade dynamics leads apparently to highly viscous flow (see Section 3.3). We have done calculations involving 2000 on 2000 nucleons and found no significant difference from the Uranium results. The momentum distribution for $b = 0$ collisions is close to an isotropic sphere. Non-viscous hydrohynamics predicts, on the other hand, a flattened pancake shape for $b = 0$ events.

The first experimental global event analysis has been completed recently.[38,39] The Ca+Ca 400 AMeV reaction has been studied in most detail, but new data on Nb + Nb is now being analyzed. The preliminary Ca data show very large fluctuations is expected. However, there is some hint[39] that cascade predicts too much transparency as compared with the data. As the new Nb data become available we can expect a much clearer experimental statement on how nuclei flow.

Finally, it is important to discuss the beam energy dependence of flow phenomena.[40] In Fig. 13, the dependence of the aspect ratio on bombarding energy is shown for $b = 0$ collisions. Observe the strong energy dependence below 400 AMeV that is predicted by hydrodynamics in contrast to the near constant isotropy predicted by cascade. Clearly global analysis is best performed in the energy range[35] 100-400 A MeV. For fun the result of a

hydrodynamic calculation assuming a density isomer equation of state at 100 AMeV is also shown. The results emphasize the need for a systematic study of flow phenomena with energy. In this way can we hope to extract details of the equation of state. In practice we will always see the combined effects of compression and viscosity. With the combined global analysis and chemical chemical composition studies (π multiplicities, deuteron yeilds, etc.) it may be possible to disentangle viscous effects from compression effects.

3.3 Nuclear Honey

Why does cascade not lead to strong collective nuclear flow? One possible answer is that the mean free path $\lambda \sim 1.7$ fm is not small enough. A necessary but not sufficient condition for hydrodynamic flow is that $\lambda/R \ll 1$, where R is the characteristic size of the system. For nuclei $\lambda/R \sim 1.4A^{-1/3} \approx 0.4$, 0.2, 0.1 for A = 40, 238, 2000 respectively. Thus, Ca+Ca obviously does not satisfy $\lambda/R \ll 1$. However, U+U could. In test runs[36] with A = 2000, that condition was rather well satisfied. Yet the flow was considerably weaker than predicted by non-viscous hydrodynamics. Is viscosity the key to the difference?

To test this idea we modified the Cugnon cascade in several ways. First we considered the effect of increasing the effective NN cross section artificially. For a fixed A, $\lambda/R = (\sigma_{eff}\rho\ R)^{-1}$ obviously decreases with increasing σ_{eff}. Second, we altered the scattering style. The conventional cascade style is to assume that nucleons propagate along straight line trajectories. At the point of closest approach, if the seperation, r , between two nucleons is less than $(\sigma_{eff}/\pi)^{1/2}$, then a random momentum transfer q is given to each nucleon. The q is chosen from the experimental distribution of momentum transfers at the appropriate NN cm energy. This

scattering style is referred to as stochastic because there is no correlation between $\underset{\sim}{r}$ and $\underset{\sim}{q}$. On the other hand, classically we expect

$$\underset{\sim}{q} \cdot \underset{\sim}{r} > 0 \text{ for repulsive forces} \quad , \tag{3.5}$$

$$\underset{\sim}{q} \cdot \underset{\sim}{r} < 0 \text{ for attractive forces} \quad , \tag{3.6}$$

$$\underset{\sim}{q} \cdot \underset{\sim}{L} = 0 \text{ for } \underset{\sim}{L} = \underset{\sim}{r} \times \underset{\sim}{p} \quad . \tag{3.7}$$

We therefore tried to impose a classical scattering style by requiring eq. (3.7) to be satisfied (this insures a well defined NN scattering plane). Furthermore, we assume that if $r < r_c$ then the force is repulsive, i.e., eq. (3.5) is satisfied, while for $r_c < r < (\sigma_{eff}/\pi)^{1/2}$ eq. (3.6) is satisfied. Thus, our classical style corresponds to a repulsive core and an attractive longer range force. Table 1 shows the results of the calculation for U+U at 250 AMeV for impact parameter b = 0. As σ_{eff} increases from σ_0 to $3\sigma_0$ the total number of NN collisions increases by a factor of 3 as expected using the stochastic style. However, the aspect ratio $a = \langle f_{max}/f_{min} \rangle$ increases only from 1.2 to 1.3. For non-viscous hydrodynamics a = 1.6. (Note that there is always some "numerical" viscosity in hydrodynamics due to finite difference techniques).

Thus, even though the number of collisions per particle, n_{coll}, increased from 5.7 to 16.5, the cascade did not reach the hydro limit. This again underscores the fact that $\lambda/R \ll 1$ is not sufficient for hydrodynamic flow. Now if we impose the classical repulsive style $r_c = (\sigma_{eff}/\pi)^{1/2}$, then as σ_{eff} increases from σ_0 to $3\sigma_0$, the aspect ratio increases from 1.3 to 2.1. Thus, we can make cascade flow even more than hydrodynamics by imposing a large repulsive classical scattering style. Note that by switching

from stochastic to repulsive style for $\sigma_{eff} = 3\sigma_o$, the total number of NN collisions decreases by a factor of two while the aspect ratio increases by a factor 1.6! This phenomenon is also clearly seen for $\sigma_{eff} = 2\sigma_o$ where we explored the dependence of n_{coll} and a on r_c. For purely repulsive style $f = r_c/(\sigma_{eff}/\pi)^{1/2} = 1$, $n_{coll} = 6.6$, $a = 1.7$. For $f = 0.5$, $n_{coll} = 18$ but $a = 1.3$! Note that for $f = 0.44$, n_{coll} has climbed to 46 collisions per incident nucleon but the aspect ratio has lowered to 1.2 (consistent with a sphere sampled with 238 particles). Therefore, increasing the attractive scattering component increases n_{coll} and lowers a.

These results can be understood as follows: the attractive scattering style tends to bring the nucleons closer together because of the focusing condition, $q \cdot r < 0$. The higher density tends to increase n_{coll}. That the aspect ratio decreases follows because transverse momentum gradients are effectively damped if $\underset{\sim}{q} \cdot \underset{\sim}{r} < 0$. This is illustrated in Fig. 14. Consider a fast stream of nucleons moving parallel to a slow stream. If the scattering style is attractive, then fast nucleons will be drawn into the slow stream and vice versa. Thus, slow and fast nucleons will mix and the transverse momentum gradient is damped. This is how usual viscosity works. However, usual viscosity increase with increasing mean free path, i.e., decreasing σ_{eff}! The viscosity effect seen in Table 1 arises out of the dynamical enhancement of mixing due to attractive forces in a high density domain. Thus, the effect seen in Table 1 for $\sigma_{eff} > \sigma_o$ is due to dynamic viscosity. For repulsive forces, Fig. 14 shows that $\underset{\sim}{q} \cdot \underset{\sim}{r} > 0$ inhibits mixing of fast and slow particles and thus helps maintain flow gradients.

Finally we observe that for $\sigma_{eff} \lesssim \sigma_o$, there is virtually no sensitivity to the scattering style. In this "long" mean free path limit, dynamic viscosity is replaced by simple kinetic viscosity.

Table 1. Sensitivity of Flow Characteristics to Scattering Style. Results based on Modified Cugnon Cascade Calculations[36] for $U^{238} + U^{238}$ at b = 0 and 250 AMeV.

σ_{eff}	$r_c/(\sigma_{eff}/\pi)^{1/2}$	$\underset{\sim}{q} \cdot \underset{\sim}{L}$	n_{coll}	f_{max}/f_{min}
σ_o	stochastic		5.7	1.2
	1.0	0	4.3	1.3
$2\sigma_o$	1.0	0	6.6	1.7
	0.63	0	11.3	1.4
	0.50	0	18.0	1.3
	0.44	0	45.8	1.2
$3\sigma_o$	stochastic		16.5	1.3
	1.0	0	7.7	2.1
$5\sigma_o$	1.0	0	8.6	3.0

Caption: σ_{eff} is effective NN scattering cross section;

σ_o is measured energy dependent total NN cross-sections;

r_c is repulsive core radius;

$\underset{\sim}{q} \cdot \underset{\sim}{L}$ is orientation of momentum transfer to angular momentum;

n_{coll} is the number of NN collisions per incident nucleon;

f_{max}/f_{min} is the aspect ratio from the flow tensor, eq. (3.4)

We now address the question of which scattering style is closer to reality. It appears that stochastic scattering is. There are two reasons. First, the sign of the NN force is both channel and energy dependent. Thus, the sign of $\underset{\sim}{q} \cdot \underset{\sim}{r}$ is likely to alternate in subsequent NN collisions as the parity of the relative wavefunction changes and as the sign phase shifts change as the relative energy is lowered. Second, and more important, there is quantum stochasticity. At these energies the relative angular momentum in NN collisions is low[1] $\ell \lesssim 3\text{-}5$ initially and $\ell \lesssim 1\text{-}2$ later. Hence low partial waves dominate the scattering. However, for low partial waves the azymuthal dependence of the scattering wavefunction weakens. Thus, there is no scattering plane (eq. 3.7) for S and P wave scattering! The stochastic scattering style abandons eq. (3.7) and choses the azymuth angle at random. Because of quantum effects this is then likely to be closer to reality.

Thus, quantum effects result in both types of processes depicted in Fig. 14. We conclude that nuclear flow is likely to highly viscous-somewhat like honey. The global analysis of nuclear collisions with A > 100 will tell us soon just how sweet nuclear flow really is.

4. QUARK - GLUON PLASMA PRODUCTION

In this last lecture we switch from honey to glue and enter into the sticky though exciting subject of the formation of a quark-gluon plasma in nuclear collisions. For this purpose we consider energies $E_{lab} > 100$ AGeV. The main question we address is whether high enough energy densities can be achieved to produce a quark-gluon plasma.

4.1 Critical parameters

One of the most striking predictions of Quantum Chromodynamics (QCD) is the deconfinement of hadronic matter at high energy density. This follows from

the asymptotic freedom property of QCD. The best estimates for the critical energy density, ε_c, come from Monte Carlo lattice simulations of QCD. The results from two recent calculations[41,42]) of the energy density ε versus temperature T in baryon free matter ($\rho_B = 0$) are shown in fig. 15. The dots and triangles are from Ref. (41), where an approximate treatment of quarks is included. The open circles are from Ref. 42 and correspond to pure SU(3) gluon matter. On the left-hand side, the ratio of ε to that of an ideal quark gluon plasma is plotted versus temperature for baryon density $\rho_B = 0$. The energy density of an ideal up-down-glue plasma is given by the Stephan-Boltzmann form[41-43])

$$\varepsilon_{SB}(T,\mu) = \frac{37}{30}\pi^2 T^4 + 3\,T^2\mu^2 + \frac{3}{2\pi^2}\mu^4 \qquad (4.1)$$

where μ is the chemical potential. The baryon density is given by

$$\rho_B = \frac{2}{3\pi^2}\mu^3 + \frac{2}{3}T^2\mu \qquad (2)$$

and the pressure in the plasma is simply $P_{SB} = \varepsilon_{SB}/3$.

In fig. 15, we see that for $T > T_c \sim 200$ MeV, $\varepsilon/\varepsilon_{SB} \approx 1$, and thus QCD predicts that the state of the matter is described well as an ideal plasma. For $T < T_c$ there is a rapid departure from the Stephan-Boltzmann form as confinement sets in.

The precise nature of the deconfinement transition is still under debate, but it is likely[43]) that for the SU(3) color group the transition is first order. The shaded area around the "data" points is to remind us that systematic uncertainties exist associated with the approximate treatment of quark degrees of freedom and finite lattice size corrections in present

calculations and that there is uncertainty in translating the lattice cutoff Λ_L into physical units (MeV).

Based on these and other model calculations at finite baryon density[43]), the following picture of the phase diagram of hadronic matter as a function of T and ρ_B is emerging: Above some critical energy density, ε_c, hadronic matter dissolves into an ideal quark gluon plasma state. A contour plot of the plasma energy density ε_{SB} is shown on the right side of fig. 15. Above the shaded region the actual energy density is very close to ε_{SB}. However, below that region there is a large reduction factor caused by confinement. While the technical definition of the transition temperature[43]) corresponds to $\varepsilon \sim 0.5$ GeV/fm^3, I define the critical temperature, T_c, here as the point where ε reaches ~90% of the Stephan-Boltzmann value. The critical energy density so defined corresponds to $\varepsilon = \varepsilon_{pl} \sim 2$ GeV/fm^3. For $\varepsilon \geq \varepsilon_{pl}$ the matter is essentially in a perturbative plasma phase, while below ε_{pl} there is a complicated mixed hadron-plasma phase.

4.2 Stopping Power and Longitudinal Growth

In a typical hadron-hadron collision a fraction $\eta \sim 1/2$ of the parallel momentum is lost. In terms of rapidity, y, this momentum loss corresponds to a rapidity shift[44])

$$\Delta y \approx \ln \frac{1}{1-\eta} < 1 \qquad (4.3)$$

for both hadrons. (Recall that for a particle of mass m and momentum $(p_\parallel, p_\perp)$, $p_\parallel = m_\perp \sinh y$ and $E = m_\perp \cosh y$ in terms of y, and $m_\perp = (m^2 + p_\perp^2)^{1/2}$.) Therefore, the rapidity of a particle after[45] $\nu \sim 0.65\, A^{0.3}$ <u>independent</u> collisions is

$$y(\nu) = y - \nu\Delta y \quad . \qquad (4.4)$$

We say that a particle is stopped if

$$\bar{\nu} > y/\Delta y \quad . \tag{4.5}$$

It is important to emphasize that stopping is a frame-dependent concept. If y_L is the lab rapidity ($y_L = 2y_{cm}$), then the particle stops in the nucleon-nucleon cm frame if $y_L < 2\nu\Delta y$. In terms of lab kinetic energy, $E_L = m_N(\text{ch } y_L - 1)$, eqs. (4.3-4.5) lead then to

$$E_L < \frac{0.5 \text{ GeV}}{(1-\eta)^{2\nu}} \sim 2^{2\nu-1}\text{GeV} \tag{4.6}$$

as a necessary condition for a nucleon to stop in the <u>NN center-of-mass (i.e., midrapidity) frame</u>. For ^{238}U, $\nu \approx 3.4$ so most nucleons stop in a central U + U collision in the midrapidity frame if the lab kinetic energy is less than $E_L < 56$ GeV for $\eta = 1/2$. A more refined recent estimate[46]) leads to a similar result. Of course eqs. (4.4-4.6) cease to hold for energies above which successive collisions are not independent. We shall see explicitely that for E > 100 GeV this is indeed the case because of longitudinal growth.

In order to calculate the energy density, we need to estimate the compression ρ_B upon stopping. If the nuclei are thick enough to stop a nucleon in the midrapidity frame (eq. (6)), <u>and</u> the nucleon recoil is instantaneous, then all nucleons will stop in a Lorentz contracted volume = γ_{cm}^{-1} x rest frame volume.[46] Therefore, the baryon density is at least[46]

$$\rho_B/\rho_o = 2\gamma_{cm} \approx \exp(y_L/2) \quad , \tag{4.7}$$

This leads to an energy density of at least

$$\varepsilon > 2\gamma_{cm}^2 M_N \rho_o \quad , \tag{4.8}$$

where $M_N \rho_o \approx 0.136$ GeV/fm^3. To obtain an upper bound on ρ_B consistent with baryon and four momentum conservation, we can use the Rankine-Hugoniot relation. Given an equation of state, $P = \alpha \varepsilon$, the shock compression ρ_{sh} is simply[35]

$$\rho_{sh}/\rho_o = \alpha^{-1} + (1 + \alpha^{-1})\, \gamma_{cm} \quad . \tag{4.9}$$

It is important to emphasize that eq. (4.9) is independent of the shock front thickness only as long as it is smaller than the dimensions of the system. With eq. (4.9) the energy density is then bounded by

$$\varepsilon < \varepsilon_{sh} = \gamma_{cm} M_N \rho_{sh} \quad . \tag{4.10}$$

However, ρ_B cannot increase indefinitely with γ_{cm}. There exists a characteristic proper recoil time $\tau_o \sim (1/2\text{-}1)$ fm/c for the baryon current to change in a collision. In a frame where the nucleon has rapidity y the time required for its baryon number to stop is dilated to τ_o ch y. Therefore, the minimum stopping distance in the mid rapidity frame is $\sim \gamma_{cm} \tau_o$. We can also think of $\gamma_{cm} \tau_o$ as the minimum thickness of any shock front in the midrapidity frame. This leads to a bound on the compression

$$\rho_B/\rho_o \lesssim g\, R/\tau_o \gamma_{cm} \equiv \rho_B(\tau_o)/\rho_o \quad , \tag{4.11}$$

where $g \sim (1\text{-}2)$ is a geometrial factor depending on the detailed spacial distribution of ρ_B (z).

To obtain a better understanding of the origin of the finite recoil time τ_0, we need to discuss to concept of longitudinal growth.[47,48] Consider a hadron of mass M suffering a collision in which it is excited to a virtual state of energy $E^{*2} = p_0^{\ 2} + M^2$. We want to know how long does it take for this virtual state to decay by emitting a particle of mass m and momentum $(p_{\parallel}, p_{\perp})$. The final state has therefore an energy $E = [(p_0 - p_{\parallel})^2 + M_{\perp}^2]^{1/2} + [\ p_{\parallel}^2 + m_{\perp}^2]^{1/2}$, where $m_{\perp}^2 = p_{\perp}^2 + m^2$ and $M_{\perp}^2 = p_{\perp}^2 + M^2$. The uncertainty principle states that the amplitude to emit such a particle becomes appreciable only for times[47]

$$t > t(y) \sim \frac{\hbar}{E^* - E} \xrightarrow[p_0 >> M]{} 2p_{\parallel}/m_{\perp}^2 = \frac{2}{m_{\perp}} \cosh y \qquad (4.12)$$

As the rapidity of the emitted particle increases, t increases because of time dilation. We can interpret eq. (4.12) as follows[48]): in the rest frame of the produce particle it takes $2/m_{\perp} \sim 1$ fm/c for the particle to come on shell. Before that time it is impossible to disentangle the wavefunction of the final particle from that of the projectile. Since the projectile is assumed highly relativistic (c = 1), the position where the particle is emitted is $z(y) \sim t(y)$. A more detailed estimate of z(y) can be made by invoking the inside-outside cascade (IOC) picture of particle production[48]). In IOC particles follow classical trajectories, $z = t \times \tanh y$, but come on shell only at $t = t(y)$. For $t < t(y)$ they propagate as virtual particles with phases interlocked with the projectile. Only for $t > t(y)$ can they participate in incoherent interactions. In this IOC picture the point where a secondary particle comes on shell is thus

$$z(y) = \frac{2}{m_{\perp}} \sinh y \quad . \qquad (4.13)$$

Equations (4.12-4.13) imply that particles come on shell when their proper time $\tau = (t^2 - z^2)^{1/2}$ reaches $\tau = 2/m_\perp \sim 1$ fm/c, i.e., along a hyperbola in the (t,z) plane. Equations (4.12-4.13) specify what is meant by longitudinal growth; at very high energies the interaction region grows very rapidly along the beam direction because of the combined effects of the uncertainty principle and relativistic kinematics.

Evidence for longitudinal growth comes from hadron-nucleus data[45,49]) as shown in fig. 16. The striking feature to observe is that for large rapidity secondaries there is virtually no dependence on the target mass, A. This is a direct consequence of longitudinal growth. A pion with rapidity y = 5 can materialize only ~100 fm downstream from the target nucleus! The absence of cascading is particularly evident when the inelasticity $\eta(\nu)$ is computed from the data ($\eta = \int dy\, dN/dy\, E(y)/E_{inc}$). We find that $\eta = 0.5$, 0.6, and 0.66 as the target changes from p, Ag, to Pb. This shows that the total energy, radiated into pions increases only very slowly ($d\eta/d\nu \sim 0.07$) with ν, in complete disagreement with the naive independent scattering model, eq. (4.4). On the other hand, models[49]) incorporating nuclear transparency and longitudinal growth have been, on the whole, successful in accounting for high energy hadron-nucleus data. Note finally that the modification of the stopping distance proposed in eq. (4.11) is consistent with the longitudinal growth of the reaction zone.

Therefore, the finite recoil time τ_0 in eq. (4.11) arises from the requirement that in the rest frame of the nucleon it takes $\tau_0 \sim 1$fm/c to radiate a pion and that this time is dialated in any other frame. Of course, it is possible to contemplate other mechanisms besides soft pion emission for the nucleon to slow down. For example, we can imagine that two colliding

nucleons with cm momentum p get excited into a very massive resonance states with $M \sim p$. However, this requires enormous momentum transfers $q \sim P$. Such amplitudes are greatly inhibited by propagator and form factors. Another generic amplitude we can invision to stop a nucleon quickly is one where the incident nucleon of four momentum $(p, \underset{\sim}{p})$ decays into a nucleon with four momentum $(m_N, 0)$ and a baryon number zero fireball of four momentum $\sim(p, \underset{\sim}{p})$. This amplitude requires only a small momentum transfer and thus is not suppressed by the propagator of the exchanged quanta. Nevertheless, there must still appear a form factor suppression with $q \sim p$ as a penalty of stopping an extended object quickly. Therefore, while there is a small finite amplitude to stop a nucleon within 1 fm, the easiest way (greatest amplitude) for a nucleon to stop is through the sequential emission of low $p_\perp$ pions. This dominant amplitude, however, has longitudinal growth built in.[47] Therefore, on the average stopping requires a distance $\sim\gamma_{cm}\tau_o$ from the interaction point. This leads to eq. (4.11).

We can now estimate at what energy the maximum baryon density is likely to be achieved. As long as the shock thickness $\gamma_{cm}\tau_o$ is smaller than $R/(2\gamma_{cm})$ in the cm frame, it pays to go to higher energies according to eq. (4.9). However, for $\gamma_{cm}\tau_o > (R/2\gamma_{cm})$, shocks can no longer be maintained and eq. (4.11) implies that ρ_B begins to decrease. Thus, we expect the maximum baryon density to be achieved when

$$\gamma_{cm}\tau_o = R/2\gamma_{cm} \tag{4.14}$$

Taking R = 14 fm for the diameter of Uranium eq. (4.14) gives $\gamma_{cm} = 2.7$ and thus the kinetic energy in the lab is $E_{lab} \approx 11$ AGeV. At that point, the

density may reach $\rho_B/\rho_0 \sim 14$. At higher energies ρ_B decreases as $1/\gamma_{cm}$ until around $E_L \sim 50$ AGeV at which point transparency sets in. Beyond that point, nuclei pass through each other although they do get compressed to $\sim(4\text{-}5)\rho_0$ in the porcess.[48,44]

The energy density, in contrast to the baryon density, continues to increase with energy as we shall see in the next section.

4.3 Proper Energy Density Achieved

Because eq. (4.13) gives a one-to-one correspondence betwen the rapidity and the production point of a particle, it is possible to compute the energy deposition per unit length, dE/dz, knowing the rapidity distribution dN/dy:

$$\frac{dE}{dz} = m_\perp \cosh y \frac{dN}{dy}\frac{dy}{dz} = \frac{m_\perp^2}{2}\frac{dN}{dy} \quad , \tag{4.15}$$

where $y = \mathrm{sh}^{-1}(m_\perp z/2)$. To compute the energy density, ϵ, we must divide dE/dz by the beam area. More precisely, we should take into account the dependence of $\epsilon(z,x_\perp)$ on the transverse coordinate $x_\perp$. If we assume, as in most models, that $\epsilon(z,x_\perp)$ is proportional to the number of struck nucleons along a tube at transverse coordinate $x_\perp$, then for a central (b = 0) nuclear collision

$$\epsilon\,(z,\, x_\perp) \approx \epsilon_{max}\,(1 - x_\perp^2/R_{min}^2)^{1/2} \quad , \tag{4.16}$$

with

$$\epsilon_{max} = \frac{3}{2\pi R_{min}^2}\frac{dE}{dz} \quad . \tag{4.17}$$

In eqs. (4.16-4.17), R_{min} is the radius of the smaller nucleus. Note that $\int d^2 x_\perp\, \epsilon = dE/dz$ and that $\langle\epsilon\rangle = 2/3\ \epsilon_{max}$. Inserting $R = 1.18\ A^{1/3}$ and $\langle m_\perp\rangle \sim 0.3$ GeV, we obtain an estimate for the maximum energy density in the central region

$$\epsilon_{max} \approx 0.1 \frac{\text{GeV}}{\text{fm}^3} A^{-2/3} \, dN/dy \quad , \tag{4.18}$$

Clearly, there is at least a factor of 2 uncertainty in the conversion factor in eq. (4.18). However, eq. (4.18) allows us to estimate ϵ_{max} from measured rapidity densities.

As a first application of eq. (4.18) consider pp collisions at ISR energies where $dN/dy \lesssim 3$ for $y_{cm} \approx 0$. In that case $\epsilon_{max} < 0.3$ GeV/fm^3, which is too small to create a plasma. Even at $p\bar{p}$ collider energies[50] $dN/dy \sim 5$ is still too small on the average. The rare events with $dN/dy \sim 10$ lead to $\varepsilon \sim 1$ GeV/fm^3, but this is still below the Stephan-Boltzmann domain.

Next consider nuclear collisions. At present the only source of experimental information comes from cosmic-ray studies[51,52] .The most spectacular event observed thus far is the so-called JACEE event[52] Si + Ag at 4-5 ATeV. Over 1000 charged particles were produced with a pseudorapidity distribution shown in fig. 17.

Note that in the central region ($\eta \sim 4$), $dn_{ch}/dy \sim 200$ is observed! This leads, assuming $\langle n_{\pi^o} \rangle = \langle n_{ch} \rangle / 3$, to

$$\epsilon_{max} \text{ (JACEE)} \sim 3 \text{ GeV/fm}^3 \quad . \tag{4.19}$$

At this point it is important to ask whether this event is just a lucky accident. To answer this question we apply the color neutralization model of ref. 49, which, as was mentioned before, is consistent with hadron nucleus data. For nucleus-nucleus collisions, this predicts

$$\langle n \rangle_{AB} \, / \, \langle n \rangle_{pp} = W_p \, \nu_T \, (1 + \nu_T)^{-1} + W_T \, \nu_p \, (1 + \nu_p)^{-1} \tag{4.20}$$

where $W_p \approx A_p$ and $W_T \approx A_T\,[1 - (1- (A_p/A_T)2/3]^{(3/2)}$ are the number of wounded nucleons in the projectile and target for b = 0, and ν_p, ν_T are the average number of mean free paths through the projectile and target. Taking[50]) $\langle n_{ch}\rangle \approx 0.88 + 0.44 \ln s + 0.118 \ln^2 s \approx 15$ and $W_p = 28$, $W_T = 58$, $\nu_p = 2.4$, $\nu_T = 5.0$ for b = 0, eq. (4.20) predicts $\langle n_{ch}\rangle_{SiAg} \approx 940$, which is close to the observed value. Thus, the JACEE event is not unusual in this respect. Nevertheless, the achieved energy density eq. (4.19) is well within the Stephan-Boltzmann domain!

A more systematic study of the energy density in the central region is shown in fig. 18. We have included the 15 high energy cosmic-ray events tabulated in ref. 52. In addition, the theoretical expectations, based on the color neutralization model for a variety of systems are also shown. For these estimates[53]), we have divided the transverse geometry into independent tube-tube collisions and applied eq. (4.20) to each tube separately. We assumed for simplicity that $dN/dy \approx \langle n\rangle/y_{cm}$ for $y_{cm} = 0$, as appropriate for the rough triangular distributions observed[52]) in nuclear collisions (see also fig. 17). The plotted curves are for the max energy density at $\tau = 1$ and $x_\perp = 0$ for b = 0 in the midrapidity frame.

It is remarkable that within the factor of 2 uncertainties in the theoretical curves, the available data are consistent with expectation. We interpret fig. 18 as experimental indication that high enough energy densities can indeed be obtained in nuclear collisions to probe the quark-gluon plasma domain. For Si + Ag the threshold for $\epsilon_{central} > \epsilon_{pl}$ seems to occur ~1 ATeV, while for U + U E_{lab} ~ 100 AGeV seems sufficient in the midrapidity region.

Now let us return to the fragmentation regions. For $E_{lab} > 100$ AGeV the baryons are certainly not stopped. However, compression caused by recoil and "slow" pion rescattering can lead to high energy densities[48]). An estimate for ϵ_{Frag} can be obtained as follows: only pions with small enough relative rapidity $y_c(A)$ can rescatter within the target or projectile nuclei. Specifically, we must have $z(y) < 2R_A$ for the pion to be produced and interact within the target nucleus. From eq. (4.13) this means that

$$y_c(A) = \sinh^{-1} m_\perp R_A \lesssim 3 \quad . \tag{4.21}$$

Therefore, the maximum energy density achieved in the fragmenation regions for $y_{Lab} > 6$ is given approximately by eq. (4.18) with dN/dy evaluated at $y_{cm} = y_{lab/2} - y_c(A)$. In fig. 19 results of calculations incuding nuclear recoil energies along the lines of ref. 44 are shown. A triangular rapidity density has been assumed. These results are in accord with earlier results[48]) where $\epsilon_{Frag} \sim 2$ GeV/fm^3 was obtained for U + U.

Also shown in Fig. 19 are estimates of the energy density in the stopping range. For these estimates we used the following interpolation formula

$$\epsilon_{stop} \sim \gamma_{cm} m_n \left(\rho_{sh}^{-2} + \rho_B(\tau_o)^{-2}\right)^{-1/2} \quad , \tag{4.22}$$

where ρ_{sh} is given by eq. (4.9) and $\rho_B(\tau_o)$ by eq. (4.11). An obvious feature in fig. 19 is that the asymptotic energy densities predicted with the modified stopping scenario (that is valid for $y_{lab} < 5$, eq. (4.22)) agree within uncertainties with the estimate based on the inside outside cascade model[48]) (that is valid only for $y_{lab} > 6$). Note also that the constancy of ϵ_{Frag} with y_{lab} is expected on grounds of scaling in the fragmentation

region. In contrast, the energy density in the central region, fig. 18, continues to grow linearly with y_{Lab} because dN/dy does not scale in this energy range[50]) at $x_F = 0$.

What figs. 18,19 show is that the domain of the quark-gluon plasma is indeed accessible via nuclear collision. They do not show, of course, what experimental signatures could result from such a plasma. Several suggestions have been put forward including strangeness abundancies[54]), dilepton yields[55]), and $\langle p_\perp \rangle$ growth[56]). We suggest a new signature: fluctuations of dN/dy on an event-by-event basis. It has been observed for some time[57]) that for high energy cosmic-ray events with $E_{Lab} > 10$ AGeV there are substantial fluctuations about the mean rapidity density that exceed those expected assuming Poisson statistics. In fig. 17 there is a hint of such fluctuations in rapidity intervals $\Delta y \sim 1$. However, the most spectacular fluctuations are observed in the events discussed in ref. 58. It is also observed that the excess dN/dy fluctuations are correlated with large $p_\perp$ gamma rays (compare fig. 13b and fig. 18 in ref. 58). Could these fluctuations be related to the first order phase transition from the plasma state back into the hadronic world This speculation is fueled by a recent suggestion[59]) that seeds for fluctuations leading to galaxy formation could arise from such a phase transition soon after the Big Bang. If the transition is indeed first order, then the plasma would not simply expand but could burn or detonate as the latent heat is converted into hadronic kinetic energy. Clearly much more thought needs to be given to the dynamics of first order phase transitions. However, it could be that we are already seeing the quark-gluon phase transition in the large fluctuations of dN/dy and the correlation of those fluctuations with high $p_\perp$.

ACKNOWLEDGMENTS

Special thanks go to R.E. Gibbs, I. Otterland, H.H. Heckman, and E. Friedlander for introducing me to cosmic-ray data. Helpful discussions with L. McLerran, H. Satz, J. Kapusta, P. Danielewicz, H. Stocker, E. Remler, B. Muller, J. Kuti, L. van Hove, J. Rafelski are also gratefully acknowledged. This work was supported by the Director, Office of Energy Research, Division of Nuclear Physics of the Office of High Energy and Nuclear Physics of the U.S. Department of Energy under Contract DE-AC03-76SF00098.

REFERENCES

1. S. Nagamiya, M. Gyulassy, "High Energy Nuclear Collisions," in Advances in Nuclear Physics (Plenum Pub. Corp., New York). eds. J. Negele, E. Vogt, in press (LBL-14035).
2. E. Friedlander, H. Heckmann, Lawrence Berkeley Lab preprint 13864 (1982).
3. E. M. Friedlander, et al. Phys. Rev. Lett. 45, 1084 (1980).
4. P. L. Jain and G. Das, Phys. Rev. Lett. 48, 305 (1982).
5. H. B. Barber, et al., Phys. Rev. Lett. 48, 856 (1982).
6. E. M. Friedlander, et al., Lawrence Berkeley Lab preprint LBL-10573 (1982).
7. B. F. Bayman et al. Phys. Rev. Lett. 49, 532 (1982).
8. A. P. Balachandran, et al. Phys. Rev. Lett. 49, 1124 (1982).
9. J. Boguta, to be published.
10. A. De Rujula et al., Phys. Rev. D17 285 (1978), D22, 277 (1980).
11. H. Georgi, Phys. Rev. D22 225 (1980).
12. R. Slansky et al. Phys. Rev. Lett 47 887 (1981).
13. R. Saly et al. Phys. Lett. 115B, 239 (1982).
14. B. Price, W. Heinrich, private communication; W. Heinrich et al., Univ. of Siegen preprint S-I-82-15 (1982).
15. A. Casher et al., Phys. Rev. D20, 179 (1979).
16. E. Kolb et al., UC Santa Barbara preprint NSF-ITP-81-66.
17. A. B. Migdal, Rev. Mod. Phys. 50, 107 (1978).
18. M. Gyulassy, W. Greiner, Ann. Phys. 109, 485 (1977).
19. M. Gyulassy, Nucl. Phys. A354, 395c (1981).
20. B. Banerjee, N. K. Glendenning, M. Gyulassy, Nucl. Phys. A361, 326 (1981).
21. S. Nagamiya et al., Phys. Rev. Lett. 48, 1780 (1982).

22. See J. Delorme, H. Toki, W. Weise, in Lecture Notes in Physics 137, Proceedings of Bologna Workshop, Nov. 25 (1980), ed. H. Arenhovel and A. M. Sarius (Springer-Verlag).

23. M. Soyeur, Proc. Symposium on Neutron Stars; European Physical Society's 5th General Conference, Instanbul, Sept. 1981.

24. J. R. Nix, D. Strottmann, Phys. Rev. C23 2548 (1980).

25. A. Sandoval et al., Phys. Rev. C21 1321 (1980).

26. J. Cugnon, Phys. Rev. C22, 1885 (1980).

27. H. Stocker et al., Phys. Rev. Lett 47 1807 (1981).

28. R. Stock et al., Phys. Rev. Lett. 44 1243 (1980).

29. H. Gutbrod, private communication.

30. R. Madey, private communication.

31. M. Gyulassy, K. Frankel, E. Remler, LBL-15285 (1982).

32. P. J. Siemens and J. O. Rasmussen, Phys. Rev. Lett. 42 844 (1979).

33. R. Stock et al., Phys. Rev. Lett. 49, 1236 (1982); and GSI-82-31 (1982) preprint.

34. H. Stocker et al., Nucl. Phys. A387 205c (1982).

35. H. Stocker, M. Gyulassy, J. Boguta, Phys. Lett. 103B, 269 (1981).

36. M. Gyulassy, K. A. Frankel, H. Stocker, Phys. Lett. 110B, 185 (1982).

37. J. Cugnon, J. Knoll, C. Riedel, Y. Yariv, Phys. Lett. 109B, 167 (1982).

38. H. H. Gutbrod, et al., LBL-14980 (1982), Nucl. Phys. A. in press.

39. H. Stroebele et al., GSI-82-32 preprint (1982); D. Beavis et al. to be published.

40. H. Stocker et al., GSI-82-8 preprint (1982).

41. J. Engels, F. Karsch, H. Satz, Phys. Lett. 113B (1982) 398

42. I. Montvay, E. Pietarinen, PL 110B (1982) 148; 115B (1982) 151

43. See contribution of H. Satz in these proceedings

44. M. Gyulassy, "Formation of Quark-Gluon Plasma in Nuclear Collisions", LBL-14512, to be published in proceedings of Bielefeld conference on quark matter and heavy ion collisions, May 8-16, 1982 (World Scientific Pub. Co., Singapore), eds. M. Jacob, H. Satz

45. J.E. Elias, et al., PR D22 (1980) 13

46. A.S. Goldhaber, Nature 275 (1978) 114; W. Busza, A.S. Goldhaber, Stony Brook preprint ITB-SB-82-22 (1982)

47. E.L. Feinberg, Phys. Rep. 5 (1972) 237; J. Koplik, A.H. Mueller, PR D12 (1975) 3638; A.S. Goldhaber, PRL 35 (1975) 748

48. R. Anishetty, P. Koehler, L. McLerran, PR 22D (1980) 2793

49. S.J. Brodsky, Proceedings of 1st Workshop on Ultra-Relativistic Nuclear Collisions, Lawrence Berkeley Laboratory, May 1979, LBL-8957, UC-34c, CONF-7905107, p. 419; see also A. Bialas contribution p. 63

50. UA5 Collaboration, PL 107B (1981) 315

51. JACEE Collaboration, in Proceedings of Workshop on Very High Energy Cosmic Ray Interactions, Univ. Penn., April 1982

52. I. Ottterlund, E. Stenlund, Physica Scripta 22 (1980) 15

53. M. Gyulassy, L. McLerran, H. Satz, to be published

54. J. Rafelski and B. Muller, PRL 48 (1982) 1066

55. K. Kajantie and H.I. Mietinnen, Z. Phys. C9 (1981) 341

56. L. van Hove, CERN preprint TH.3391 (1982)

57. J. Iwai, N. Suzuki, and Y. Takahashi, Prog. Theor. Phys. 55 (1976) 1537

58. J. Iwai, et al., Nuovo Cim. 69A (1982) 295

59. M. Crawford, D.N. Schramm, Nature 298 (1982) 538

60. J.D. Bjorken, Fermilab preprint Pub-82/44-THY (1982); K. Kajantie and L. McLerran, Univ. Helsinki preprint HU-TFT-82-24 (1982)

Figure Captions

Fig. 1 Mean free path of primary ^{16}O at 2.1 AGeV in emulsion as a function of distance from the scan line.[6]

Fig. 2. Two chain event[6] produced by ^{56}Fe at 1.88 AGeV in emulsion. A secondary with Z = 9 travels a distance X = 2.6 cm before interacting. A tertiary with Z = 8 then travels a distance Y = 0.02 cm before interacting. The mean free path for primaries with Z ~ 8–9 is $\lambda_{Em} \approx 10$ cm.

Fig. 3. The reduced mean free path Λ^*, eq. (2.4), as a function of distance, D, from the primary vertex. Results from three emulsion experiments[2-4] show significant dependence of Λ^* for D < 5 cm.

Fig. 4. Normalized likelihood contours[6] for fits to Fig. 3 assuming a fraction α of all secondaries have anomalous mean free path λ_a. The cross indicates the position of maximum likelihood.

Fig. 5. The ratio of the mean free path $\lambda_Q(A)$ for quark-nuclear complexes to the normal nuclear mean free path $\lambda(A)$ in emulsions is shown on top as a function of the total number of nucleons eaten by the quark. On bottom the mass per eaten nucleon is shown. Solid curves are for different bare quark masses. Dashed curves define the appetite of a quark for different interaction fudge factors. The intersectionof a dashed and solid curve gives the value of A for which $\partial M/\partial A = M_n$.

Fig. 6. Pion spectra at $\theta_{cm} = 90°$ produced in Ne + NaF 0.2-2.1 AGeV reactions.[21] An estimate[19] of the order of magnitude of the contribution due to spin-isospin current instabilities is indicated. The data at 0.2 AGeV rule out such instabilities and are consistent with simple phase space models.[21]

Fig. 7A Comparison of charge inclusive data[25] with nonviscous hydrodynamical calculations.[24] The dots are the data and the histograms are calculations. Three different equations of state were tested.

7B Comparison of data[25] with calculations[31] using the Cugnon cascade code.[26] In parts a, c charge inclusive distribution are shown. In parts b and d primodial deuteron distributions[31] are shown. The dots in b, d show free deuteron spectra.[25] Triangles include d, t, He^3, α.

Fig. 8. Angular distribution of protons with different kinetic energies (middle left)[28] are compared to two cascade calculations, two hydrodynamic calculations and a firestreak calculation as described in Ref. (27). The reaction Ne+U at 393 AMeV triggered on high multiplicity is considered.

Fig. 9a. Mean π^- multiplicity produced in central Ar + KCl collisions versus cm kinetic energy per nucleon.[33] Open circles show predictions of Cugnon cascade.[26] Triangles are data. Horizontal arrows are used to estimate of compression energy per nucleon.

9b. Compression energy deduced[33] from (a) versus baryon density as predicted by the cascade code. Dashed curves illustrate an equation of state with incompressibility constant K = 200 - 250 MeV.

Fig. 10. The trajejctories $T(\rho)$ followed in hydrodynamical compression and expansion[34] at energies 0.2, 0.4, 0.8 AGeV. Shaded area indicates temperature increase due to viscosity. A linear (ρ) and quadratic (ρ^2) dependence of the compression energy per nucleon is contrasted.

Fig. 11. Ratio of average π^- multiplicity to proton multiplicity is shown for fireball model (dotted line), non-viscous hydrodynamics (η = 1.0), and viscous hydrodynamics (η = 1.15, 1.22). Data[33] are shown by dots.

Fig. 12. Kinetic flow diagram for U + U at 400 AMeV. The flow angle is the angle between the beam axis and the principal axis carrying the largest kinetic energy. The ratio of the largest ,a, to smallest ,b, eigen values of the tensor specify the aspect ratio of the event. Numbers indicate impact parameter in units of $b_{max}/10$. The solid curve is prediction of non-viscous hydrodynamics.[40] Shaded region is predition of cascade.[36] Insert shows the flow analysis of one Ca+Ca (400 AMeV) event meausred in the plastic ball.[38]

Fig. 13. Energy dependence of the kinetic flow ratio (f_{max}/f_{min}) for b = 0 U + U collisions. Solid line refers to hydrodynamics,[40] while shaded region refers to cascade.[36] A density isomer leads to the x at 100 AMeV.

Fig. 14. Transverse flow gradients are maintained by repulsive scattering style while they are rapidly damped by attractive scattering style.

Fig. 15. Phase diagram of hadronic matter. Monte Carlo QCD data[41-43] on left indicate existence plasma transition at energy densities ~2GeV/fm^3. Equal ϵ_{SB} contours, eq. (4.1), versus T and ρ_B are shown on the right.

Fig. 16. Pseudo rapidity (η =-ln tan $\theta_{Lab}/2$) distributions of particles produced in p + A collisions at 200 GeV.[45]

Fig. 17. Pseudo rapidity distribution[51] of Si (4 -5 ATeV) + Ag $\rightarrow$ 1000 charges + X. The most spectacular nuclear collision ever recorded! Dashed triangle is to guide the eye.

Fig. 18. Maximum energy density achieved in low baryon density regions[53] (midrapidity). Eq. (4.18) was used to convert measured multiplicities[51,52] into proper energy densities. Diamonds correspond to Si + Ag, square to Ar + Pb, open circles to "light" (α, B, C, N) + Ag collisions. Theoretical estimates for various systems are based on eqs. (4.18,4.20) using tube-tube geometry as discussed in text.

Fig. 19. Energy density achieved in high baryon density regions. Curve G illustrates eq. (4.8))). Shock curves eq. (4.22) for Stephan-Boltzmann gas ($\alpha = 1/3$), $gR/\tau_0 = 20$, 10 are given by 1 and 2. Stiff equation of a state curves 1', 2' correspond to $\rho_{sh} = 2\gamma_{cm}\,\rho_0$ and $gR/\tau_0 = 20$, 10 resp. in eq. (4.22). Curves 3, 4, 5 based on inside-outside cascade[44,48] and eq. (4.21) with $m_\perp R/2 = 5$, 10, 15 resp. Shaded area is best guess for central U + U collisions.

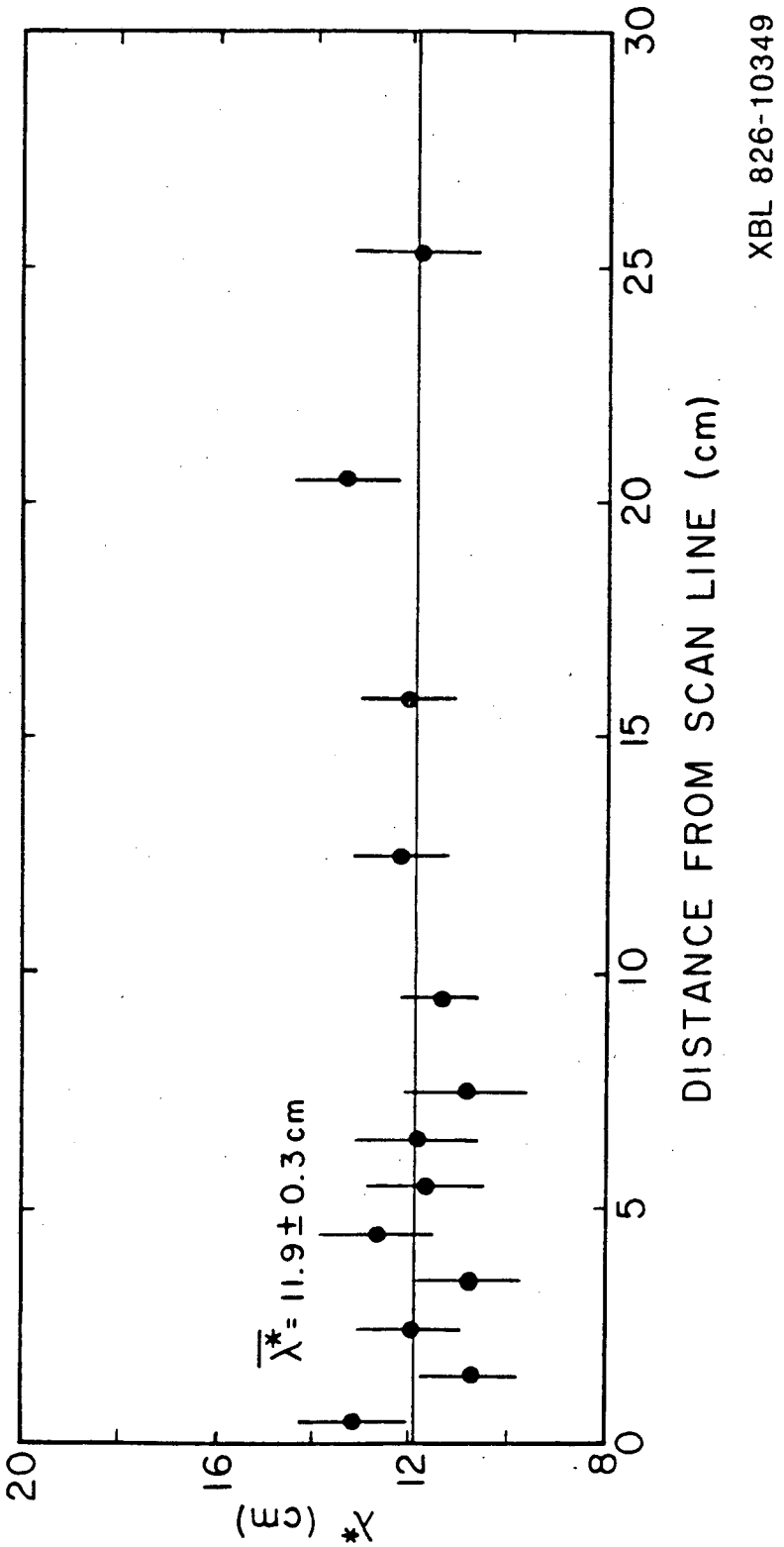

XBL 826-10349

Fig. 1

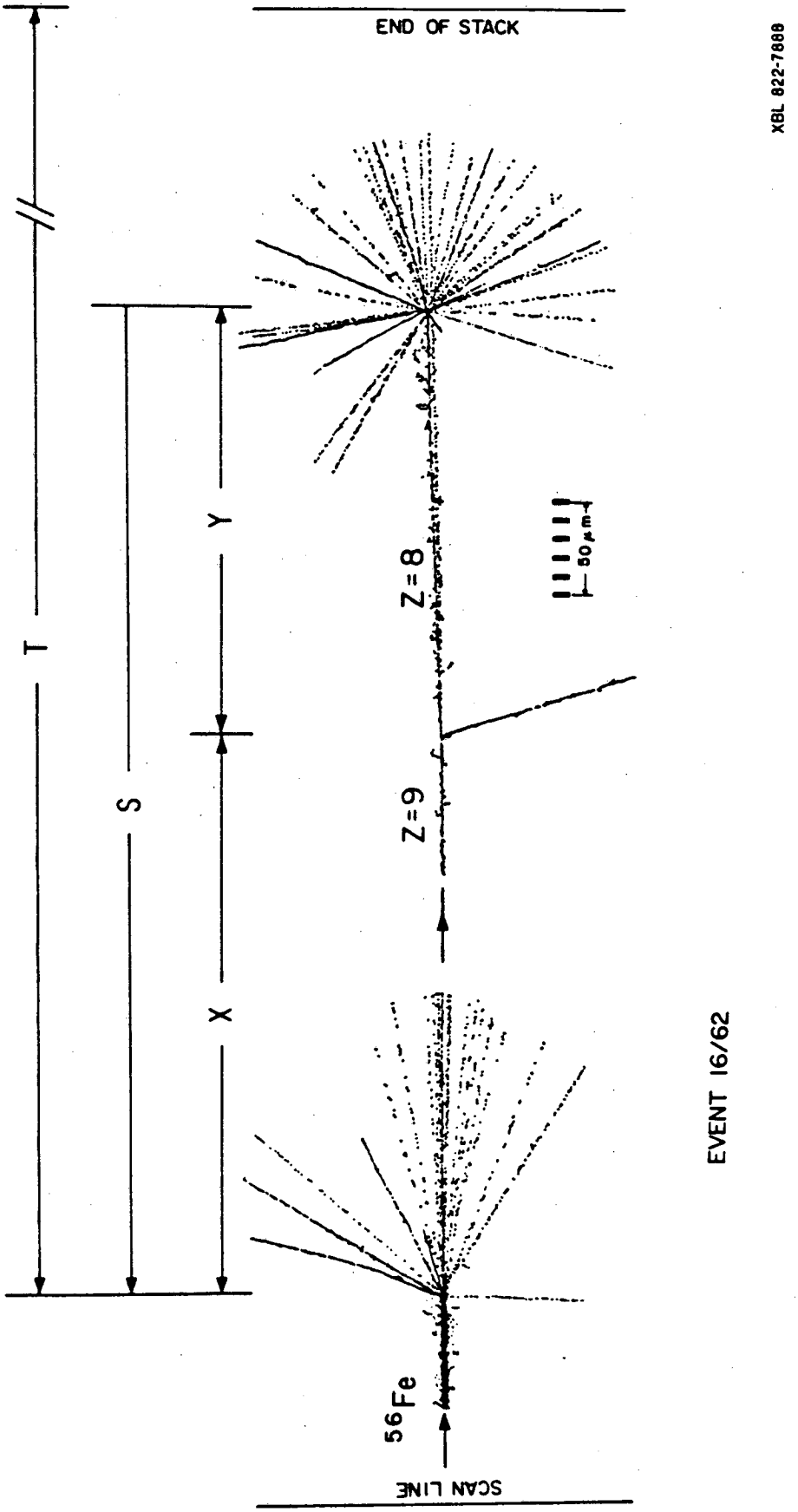
END OF STACK
T
S
Y
X
Z=8
Z=9
50 μm
56Fe
SCAN LINE
EVENT 16/62
XBL 822-7888

Fig. 2

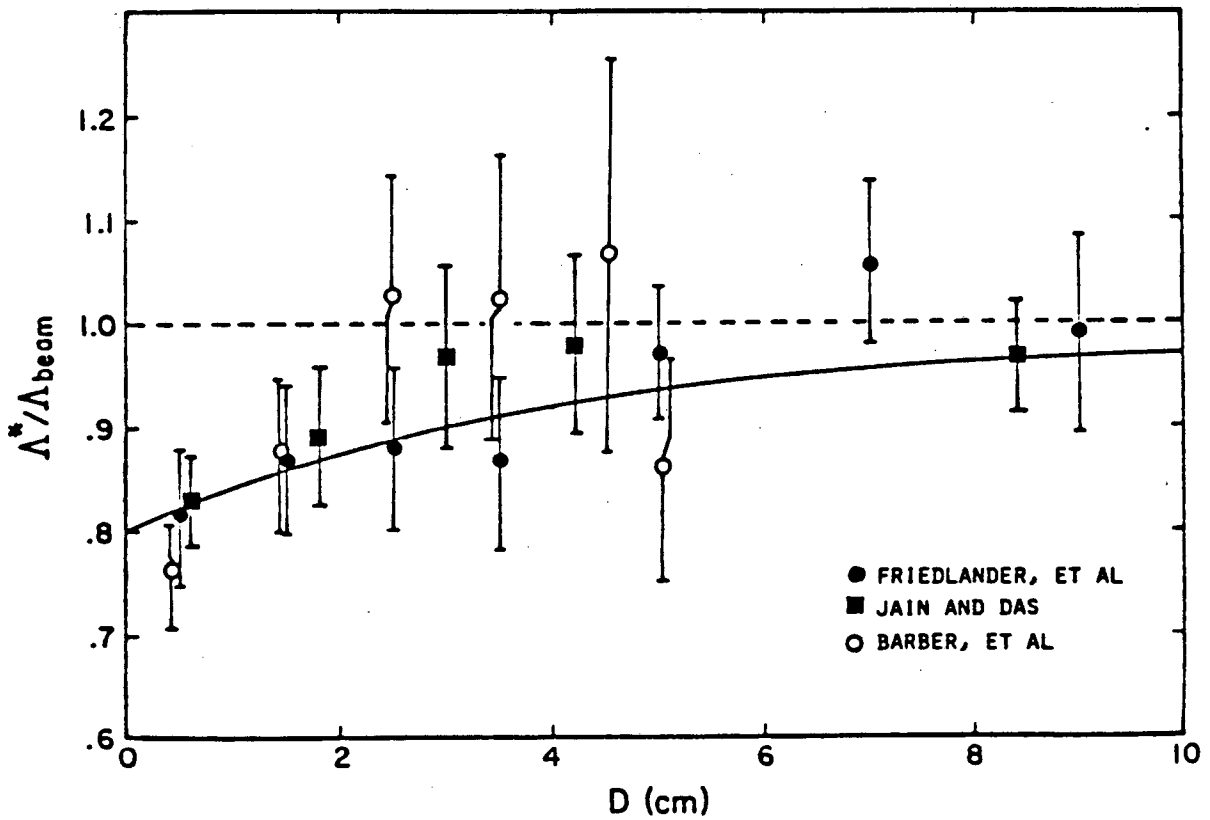

XBL 8210-3024

Fig. 3

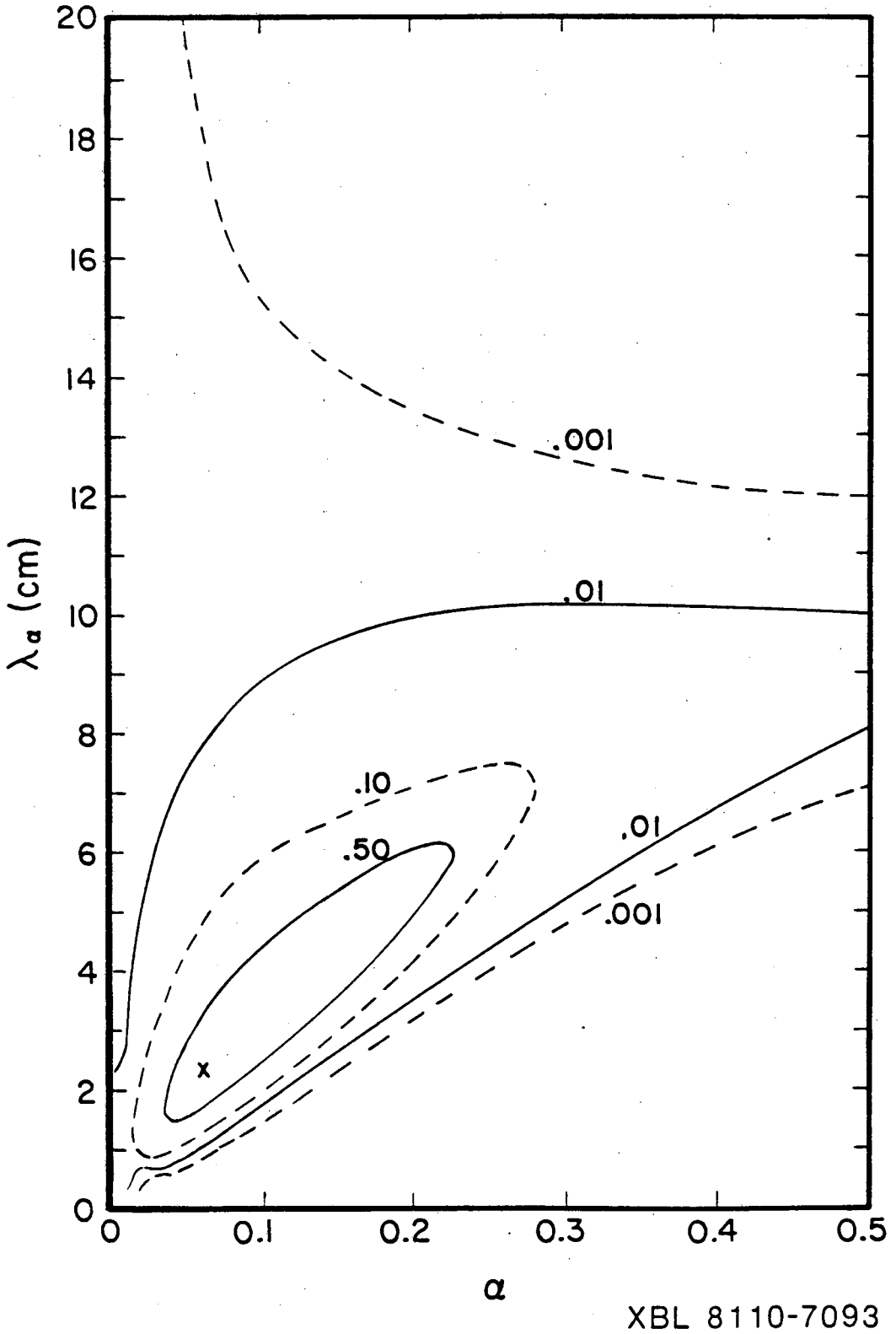
20
18
16
14
12
10
8
6
4
2
0
λ_a (cm)
0
0.1
0.2
0.3
0.4
0.5
α
.001
.01
.10
.50
.01
.001
x
XBL 8110-7093

Fig. 4

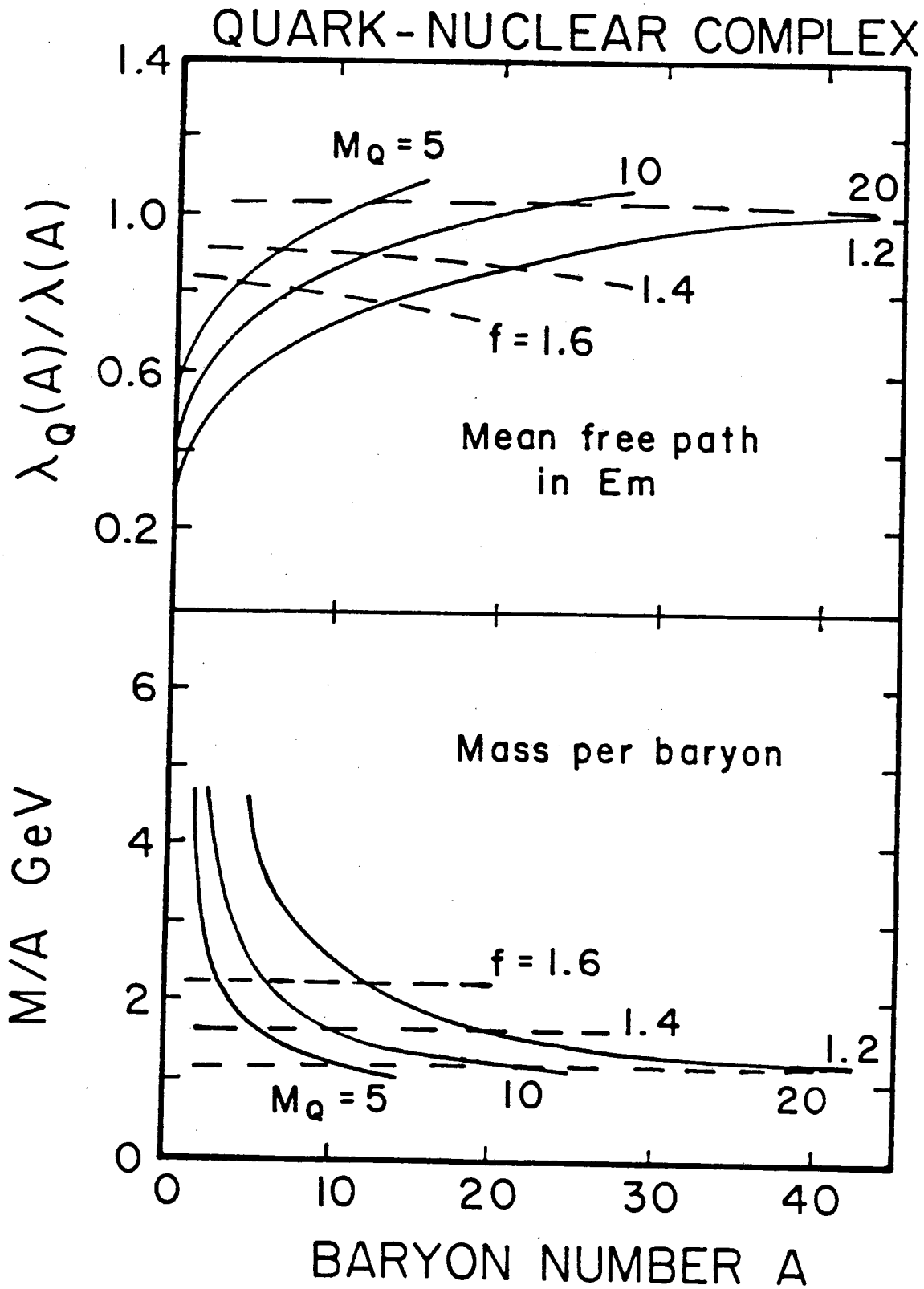

XBL 8212-11994

fig. 5

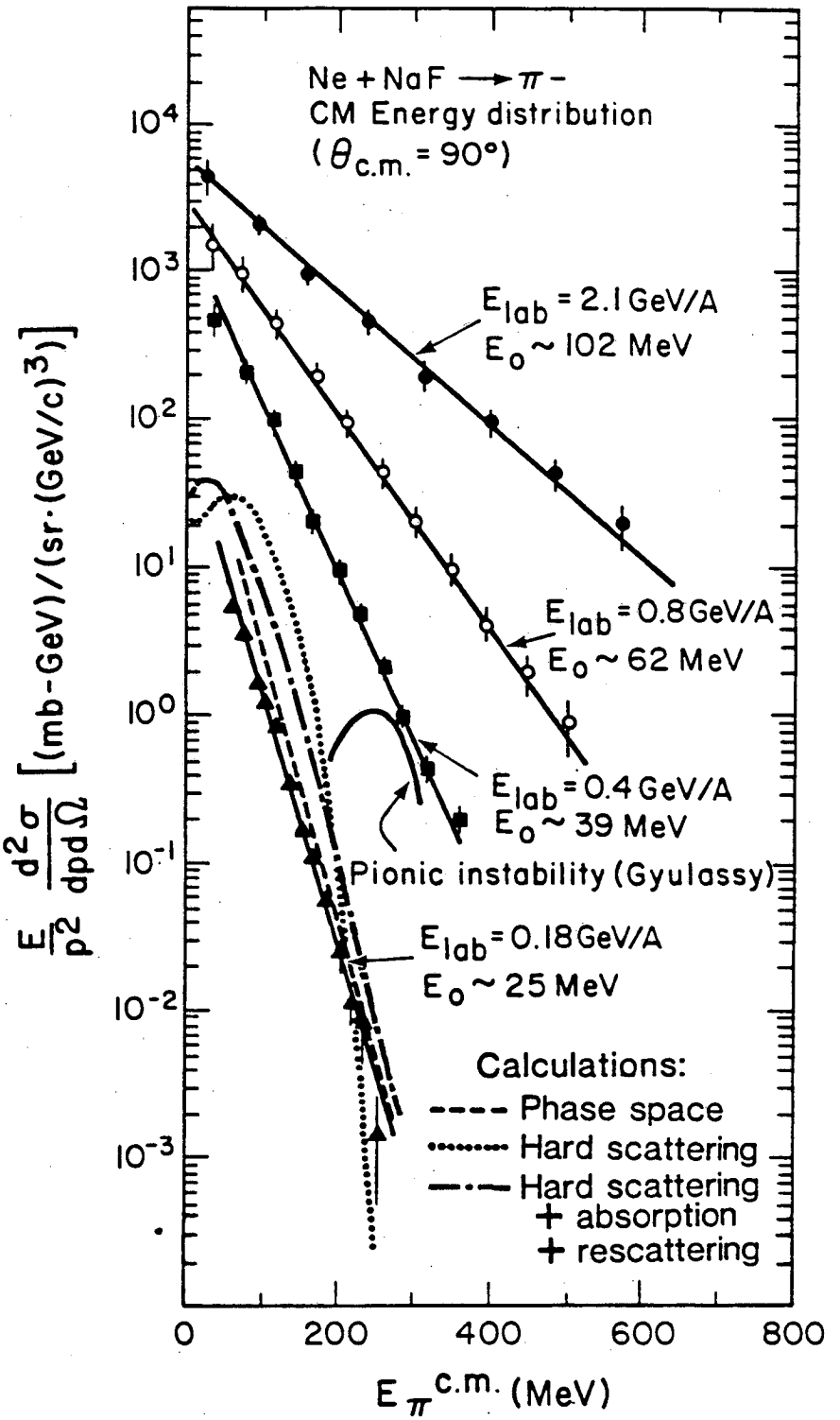

XBL 8112-13235

Fig. 6

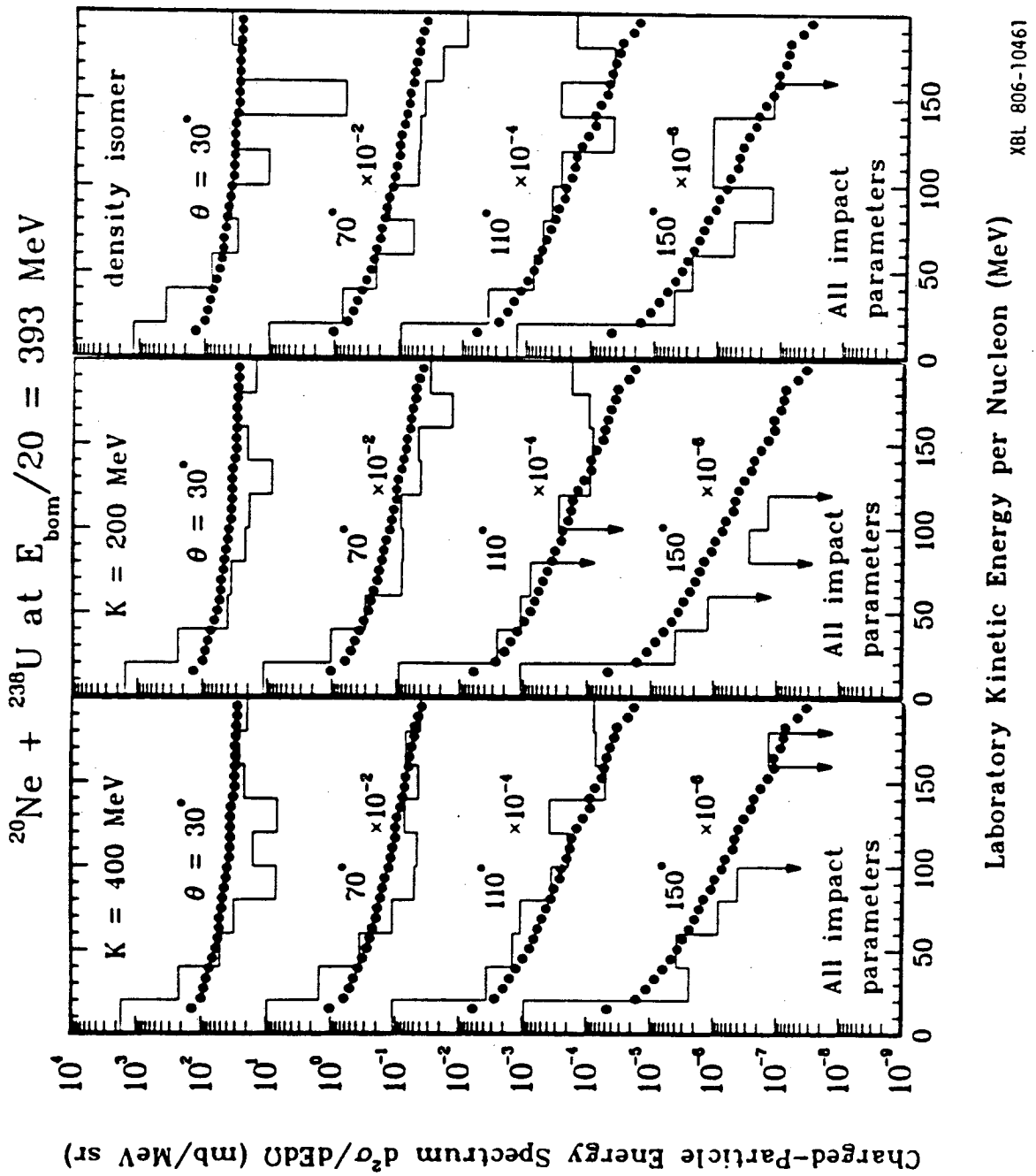
^{20}Ne + ^{238}U at $E_{bom}/20$ = 393 MeV
K = 400 MeV
K = 200 MeV
density isomer
θ = 30°
70°
110°
150°
×10⁻²
×10⁻⁴
×10⁻⁶
All impact parameters
Laboratory Kinetic Energy per Nucleon (MeV)
Charged-Particle Energy Spectrum d²σ/dEdΩ (mb/MeV sr)
XBL 806-10461

Fig. 7A

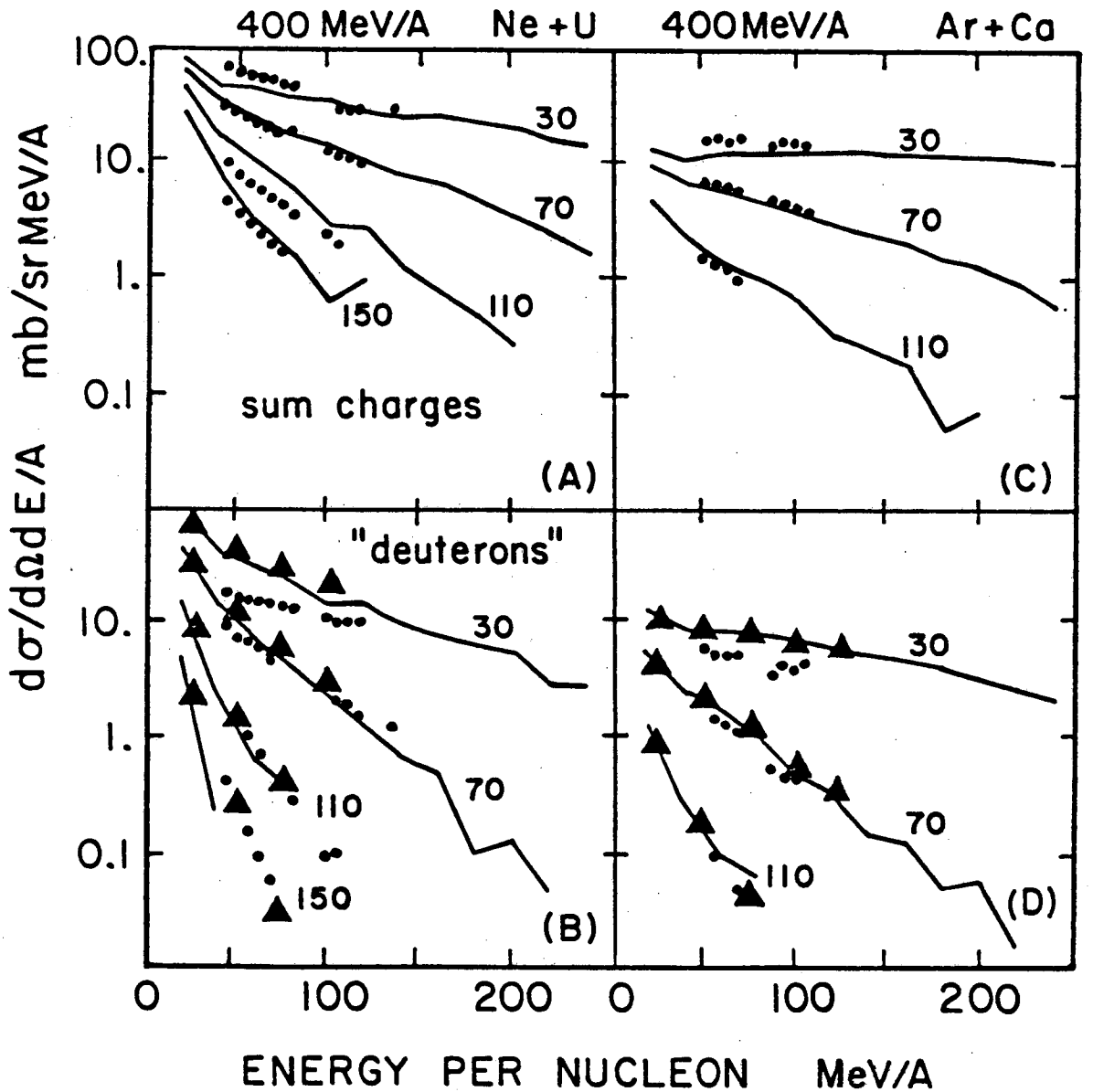

XBL 822-7955

Fig. 7B

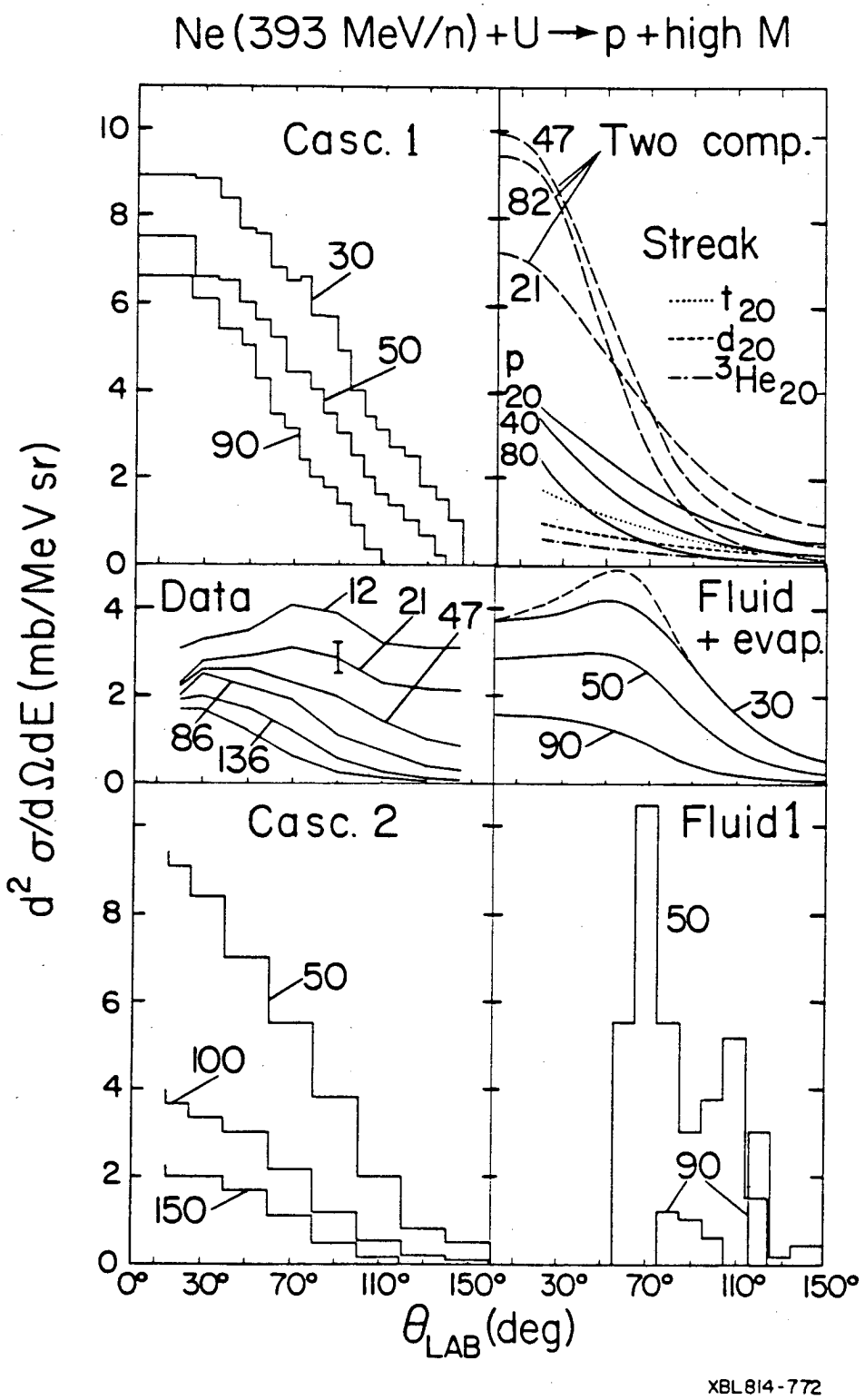
Ne(393 MeV/n)+U→p+high M
Casc. 1
30
50
90
Two comp.
47
82
21
Streak
t20
d20
3He20
p
20
40
80
Data
12
21
47
86
136
Fluid
+ evap.
50
30
90
Casc. 2
50
100
150
Fluid1
50
90
d2σ/dΩdE (mb/MeV sr)
θLAB (deg)
0° 30° 70° 110° 150° 30° 70° 110° 150°
XBL814-772

Fig. 8

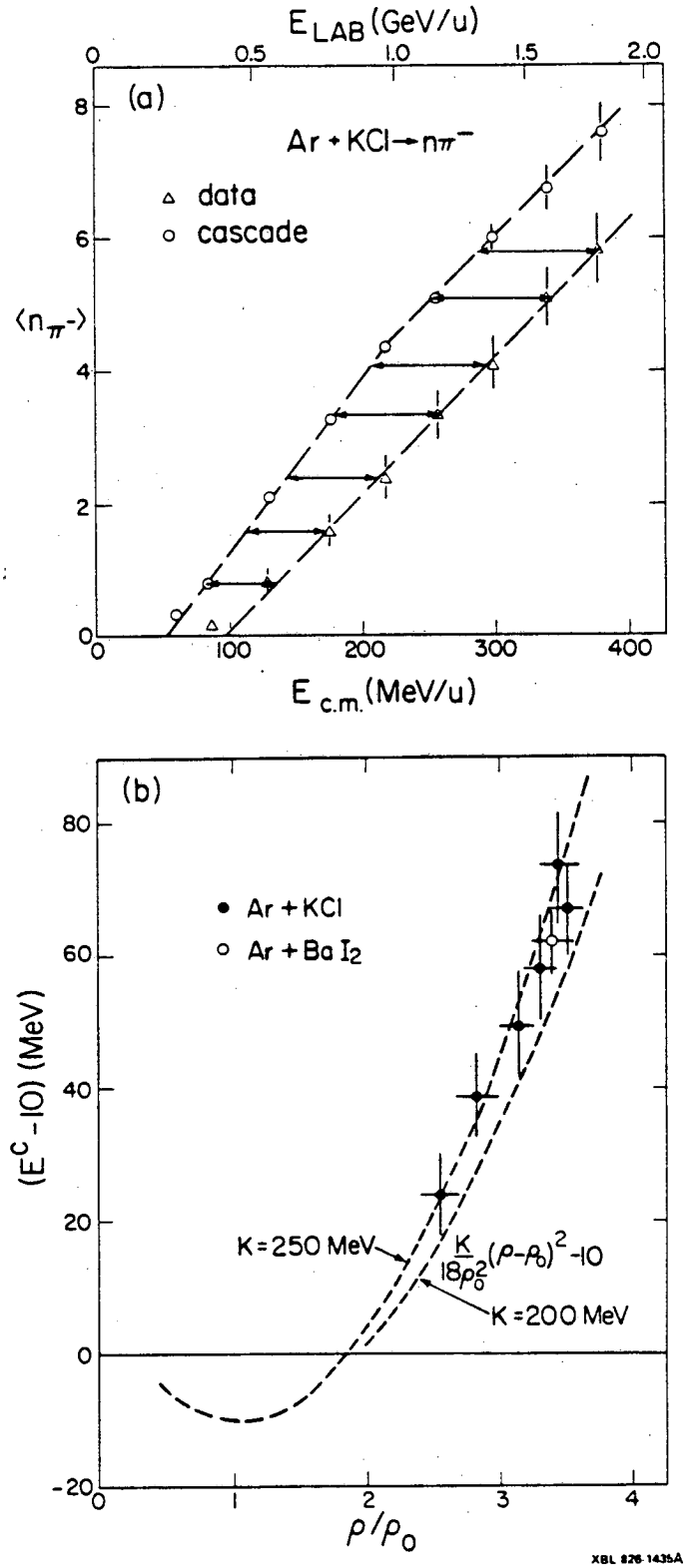
E LAB (GeV/u)
0
0.5
1.0
1.5
2.0
(a)
Ar + KCl → nπ⁻
data
cascade
⟨nπ⁻⟩
0
2
4
6
8
0
100
200
300
400
E c.m. (MeV/u)
(b)
Ar + KCl
Ar + Ba I2
(E^C - 10) (MeV)
80
60
40
20
0
-20
K = 250 MeV
K/18ρ₀² (ρ-ρ₀)² -10
K = 200 MeV
0
1
2
3
4
ρ/ρ₀
XBL 826-1435A

Fig. 9

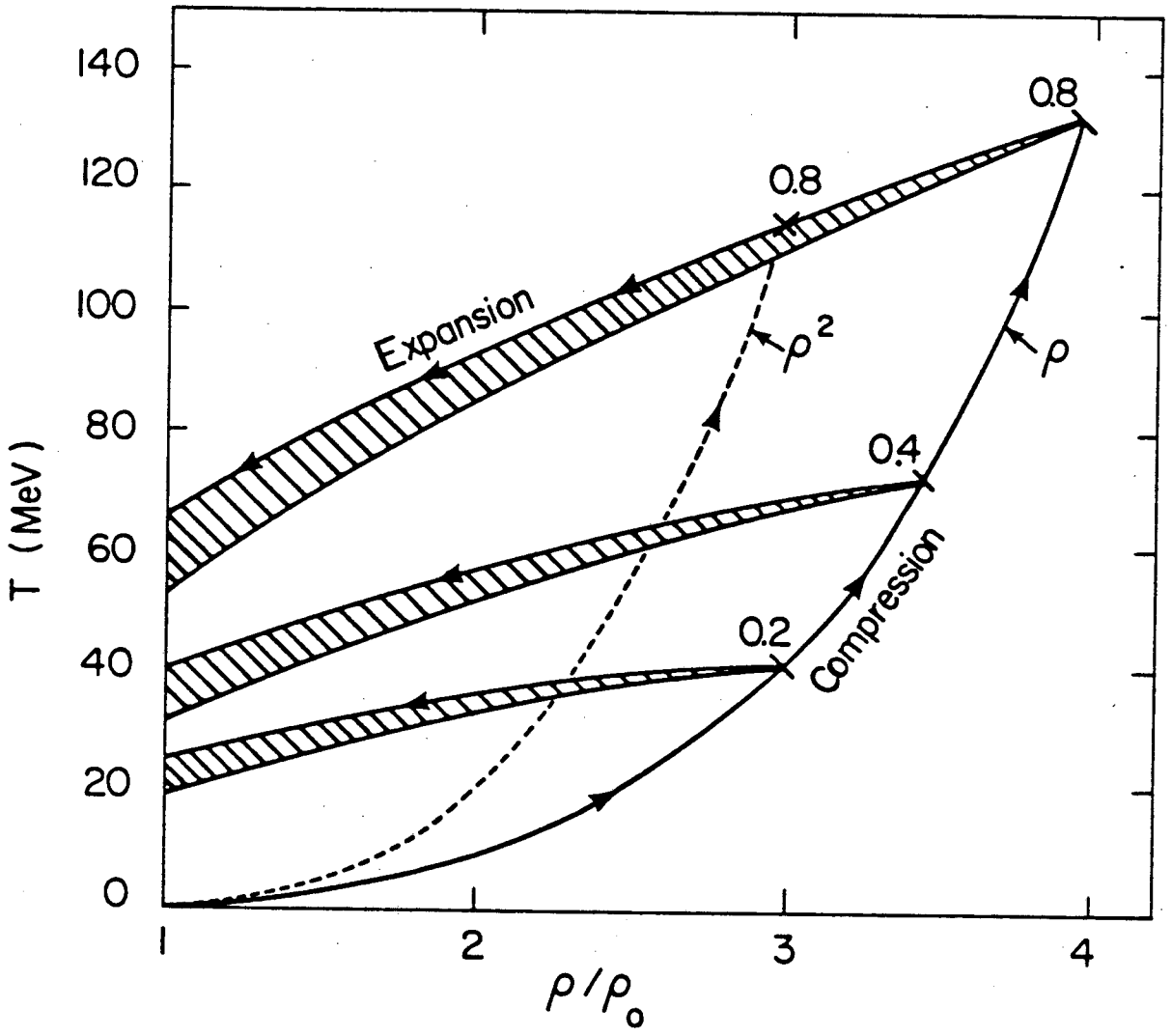

XBL 813-427

Fig. 10

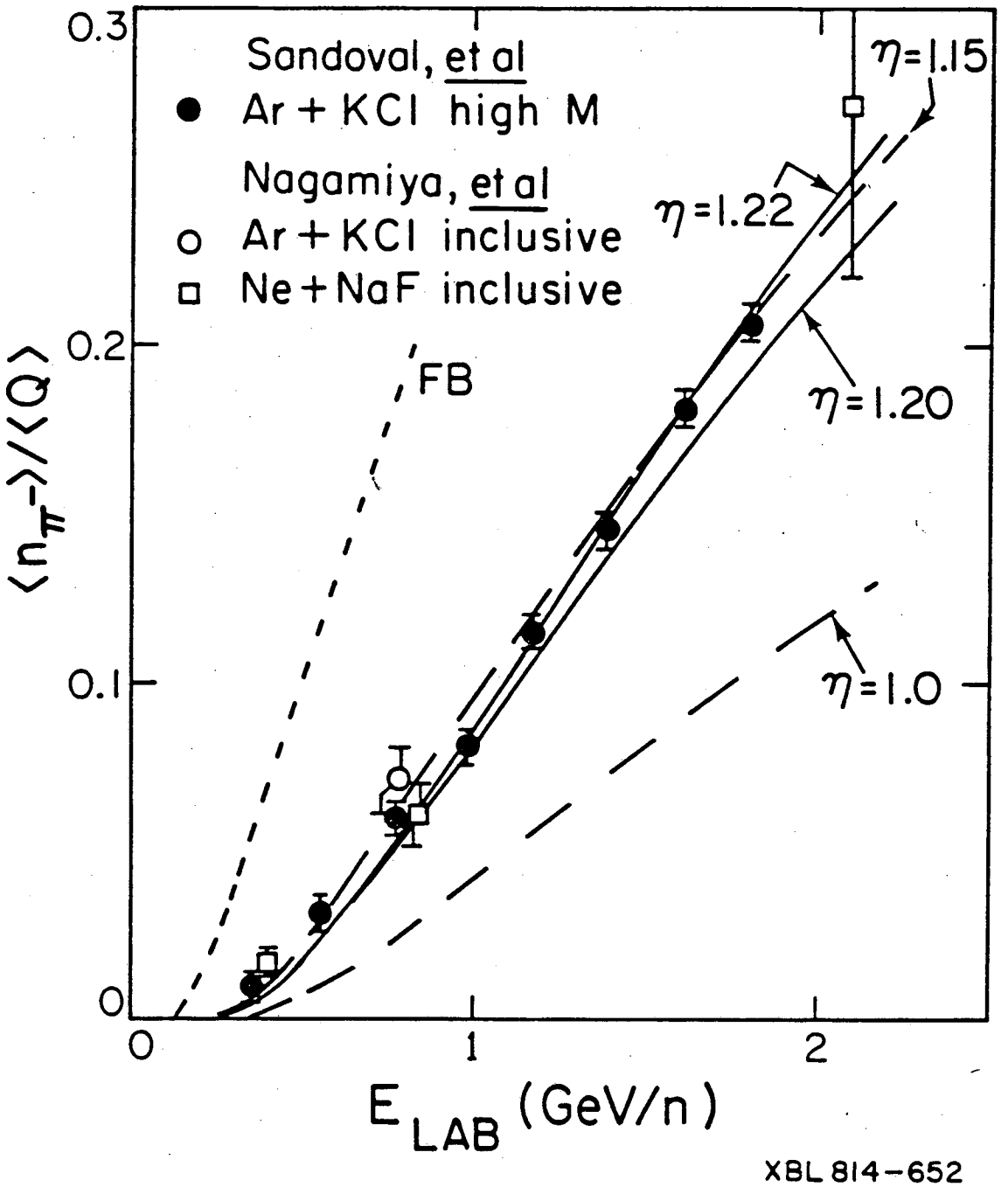
Sandoval, et al
Ar + KCl high M
Nagamiya, et al
Ar + KCl inclusive
Ne + NaF inclusive
FB
η=1.15
η=1.22
η=1.20
η=1.0
0.3
0.2
0.1
0
0
1
2
⟨n_π⁻⟩/⟨Q⟩
E_LAB (GeV/n)
XBL 814-652

Fig. 11

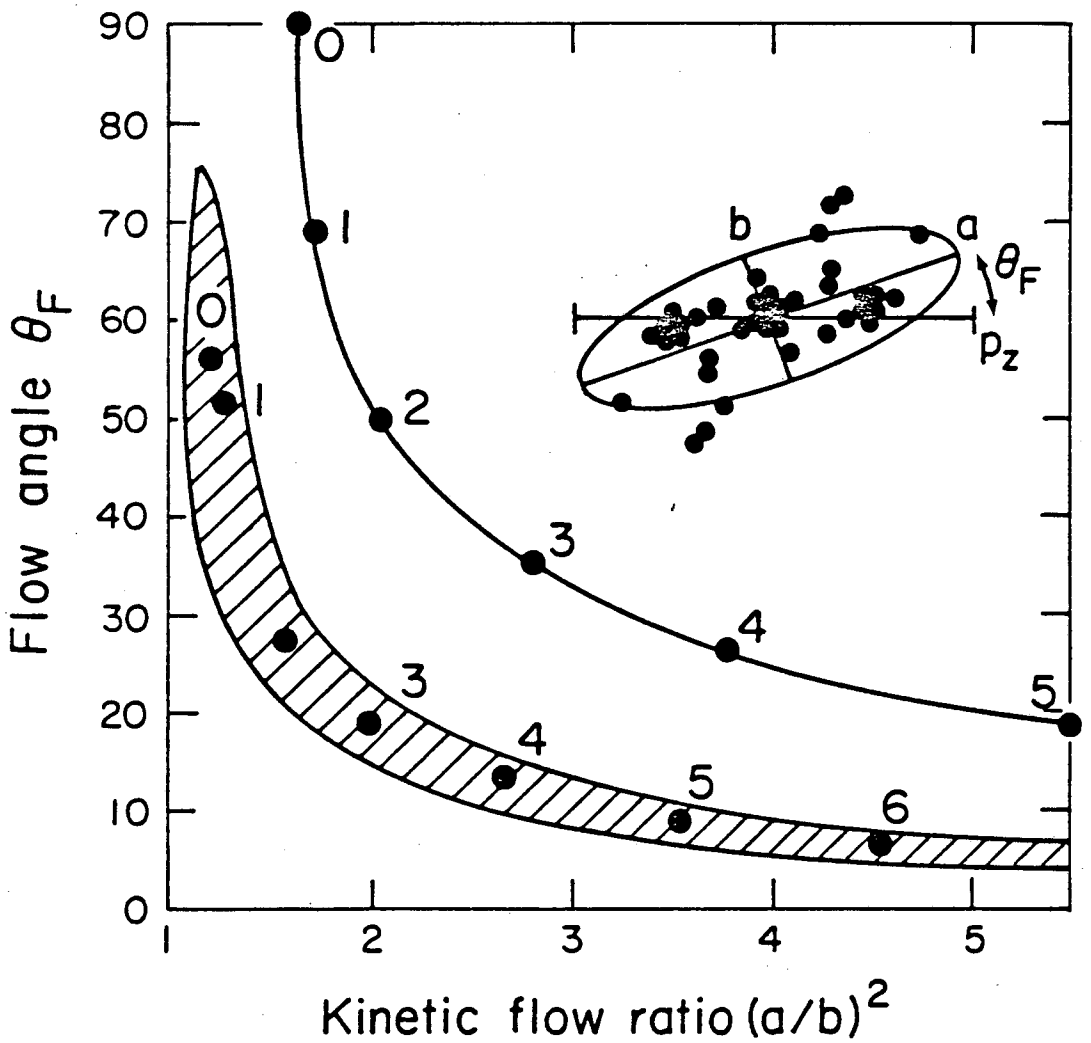

XBL 822 - 4485

Fig. 12

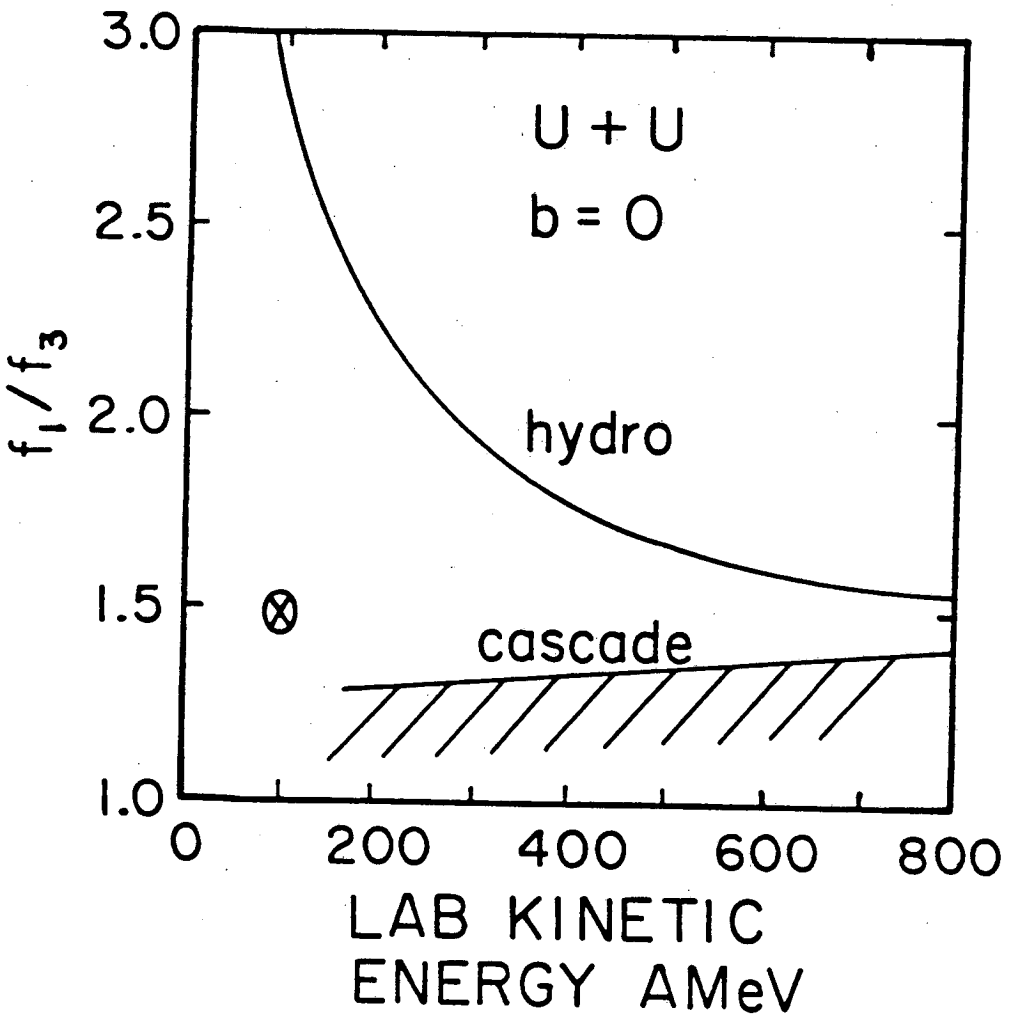

XBL 3212-12144

Fig. 13

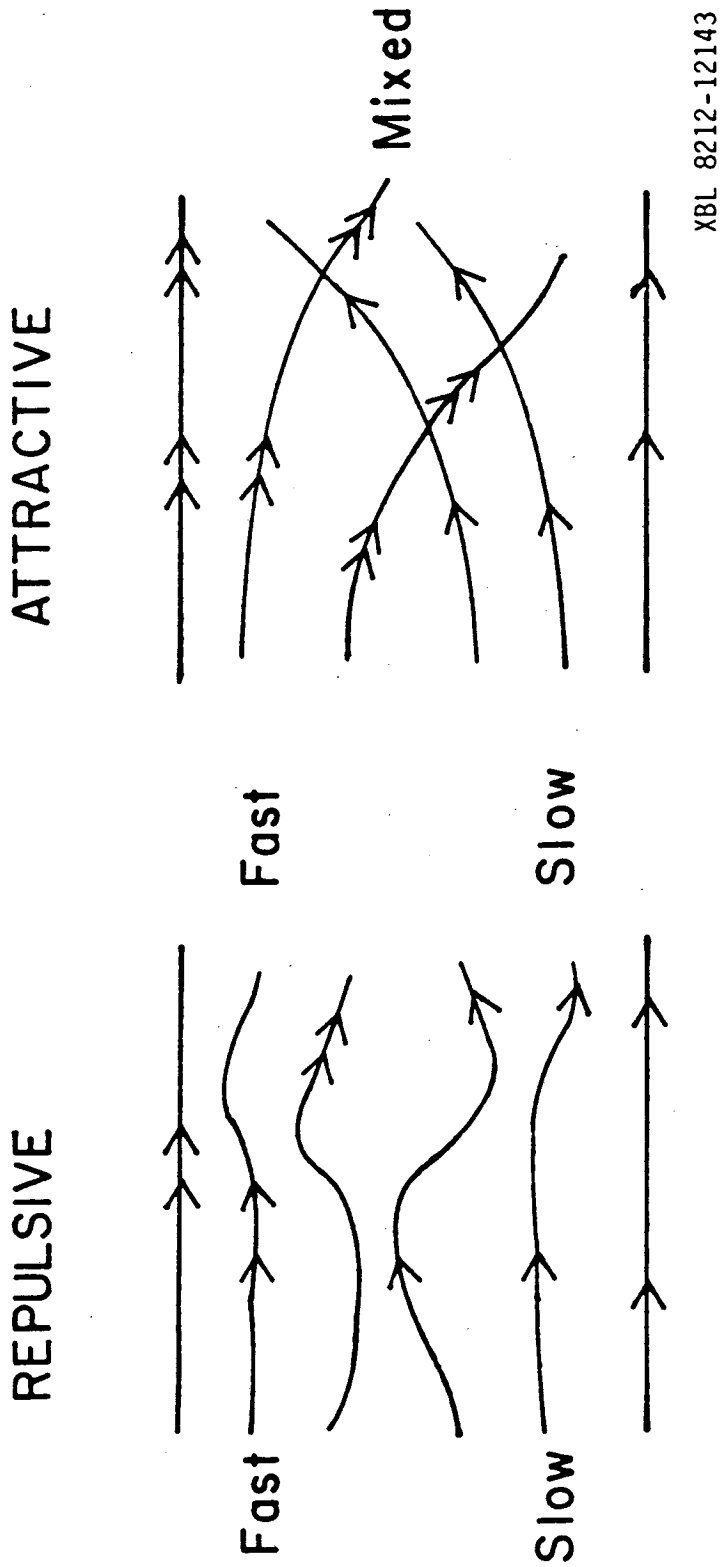
REPULSIVE
ATTRACTIVE
Fast
Slow
Fast
Slow
Mixed
XBL 8212-12143

Fig. 14

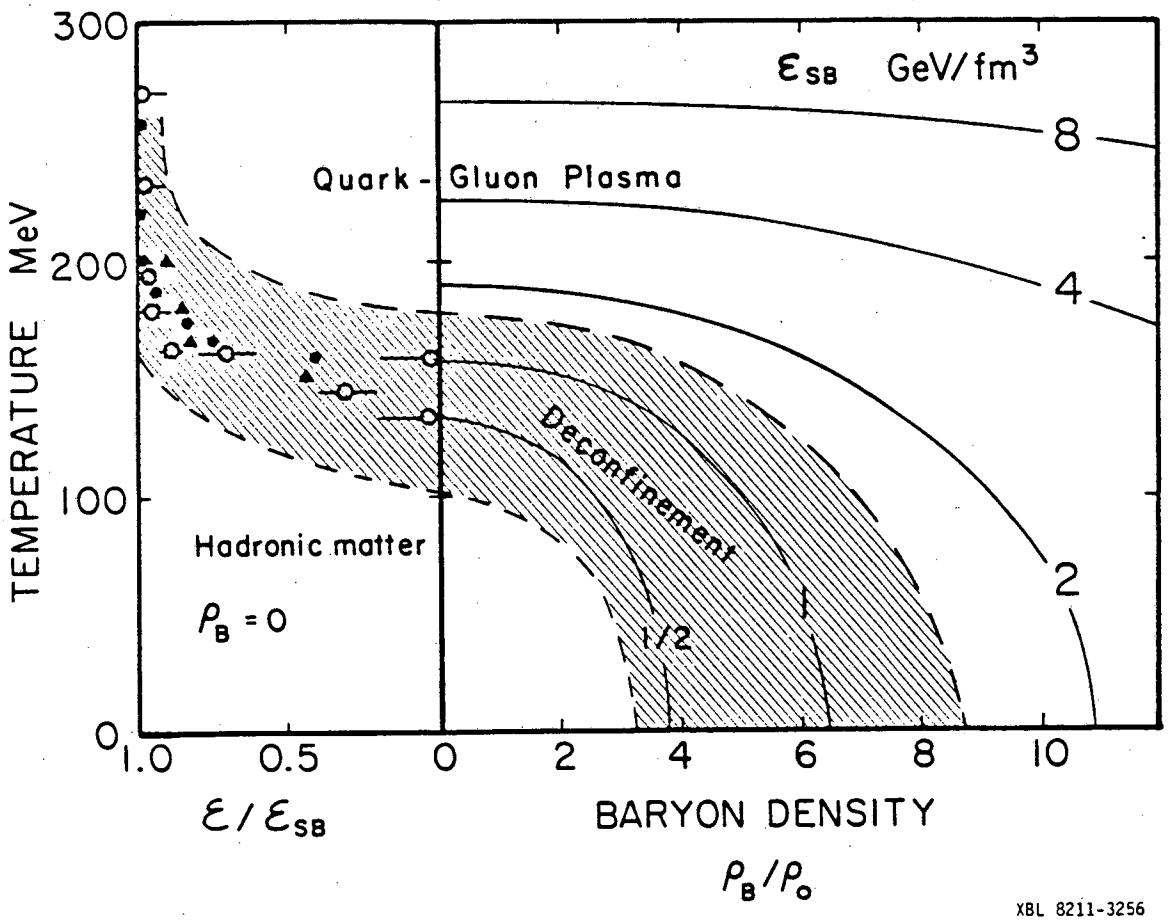
300
200
100
0
TEMPERATURE MeV
1.0
0.5
0
2
4
6
8
10
$\mathcal{E}/\mathcal{E}_{SB}$
BARYON DENSITY
ρ_B/ρ_o
$\mathcal{E}_{SB}$ GeV/fm^3
8
4
2
1
1/2
Quark - Gluon Plasma
Deconfinement
Hadronic matter
$\rho_B = 0$
XBL 8211-3256

Fig. 15

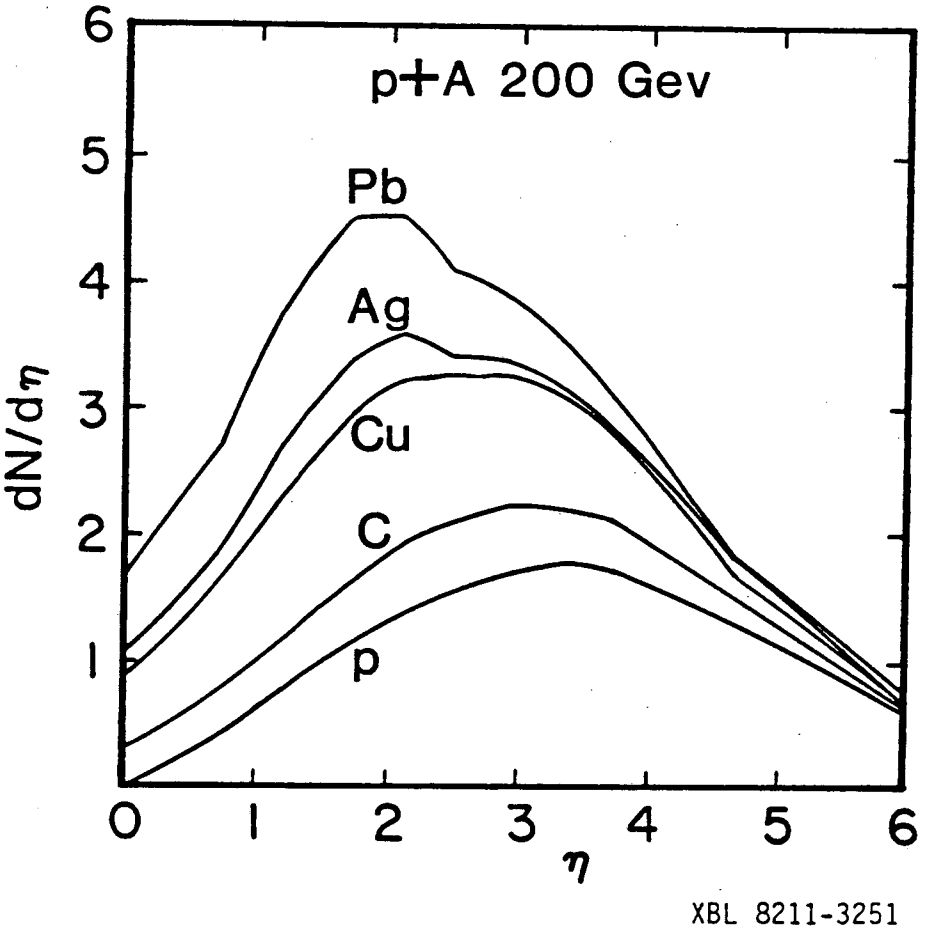

Fig. 16

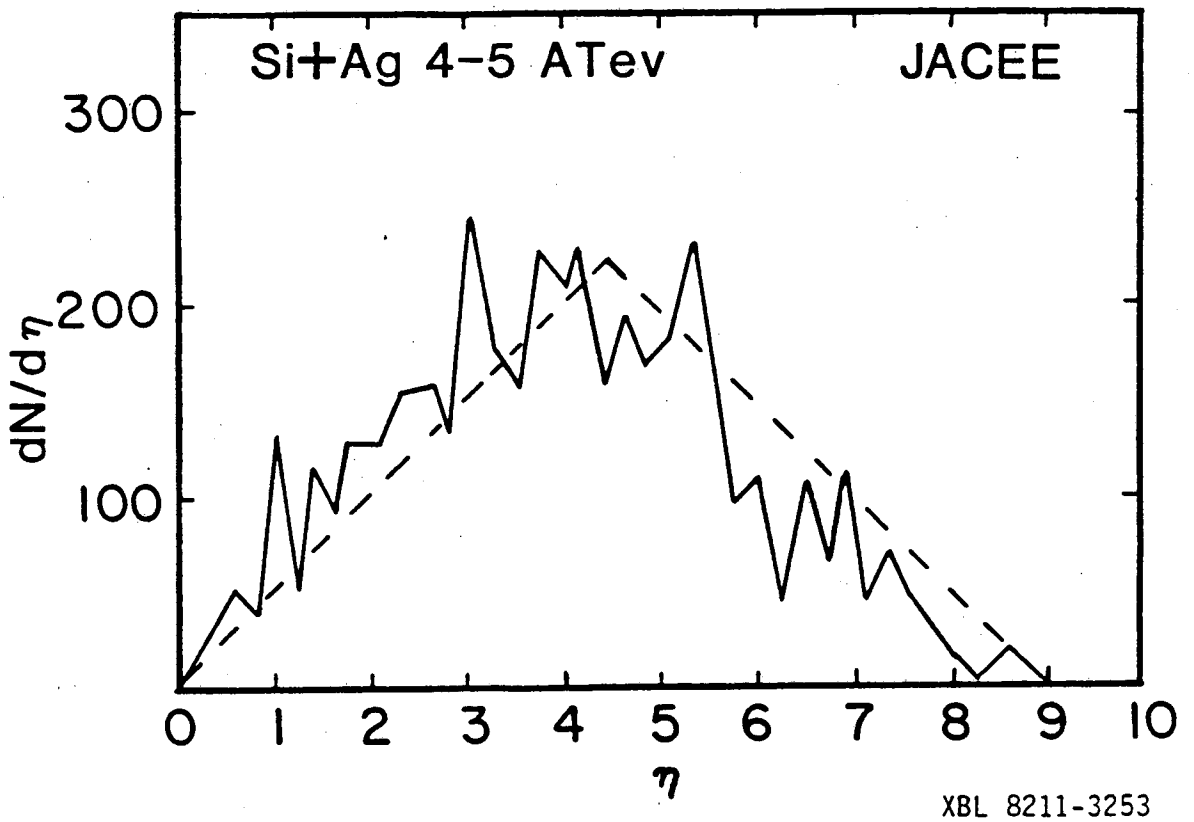
Si+Ag 4-5 ATev
JACEE
300
200
100
dN/dη
0
1
2
3
4
5
6
7
8
9
10
η
XBL 8211-3253

Fig. 17

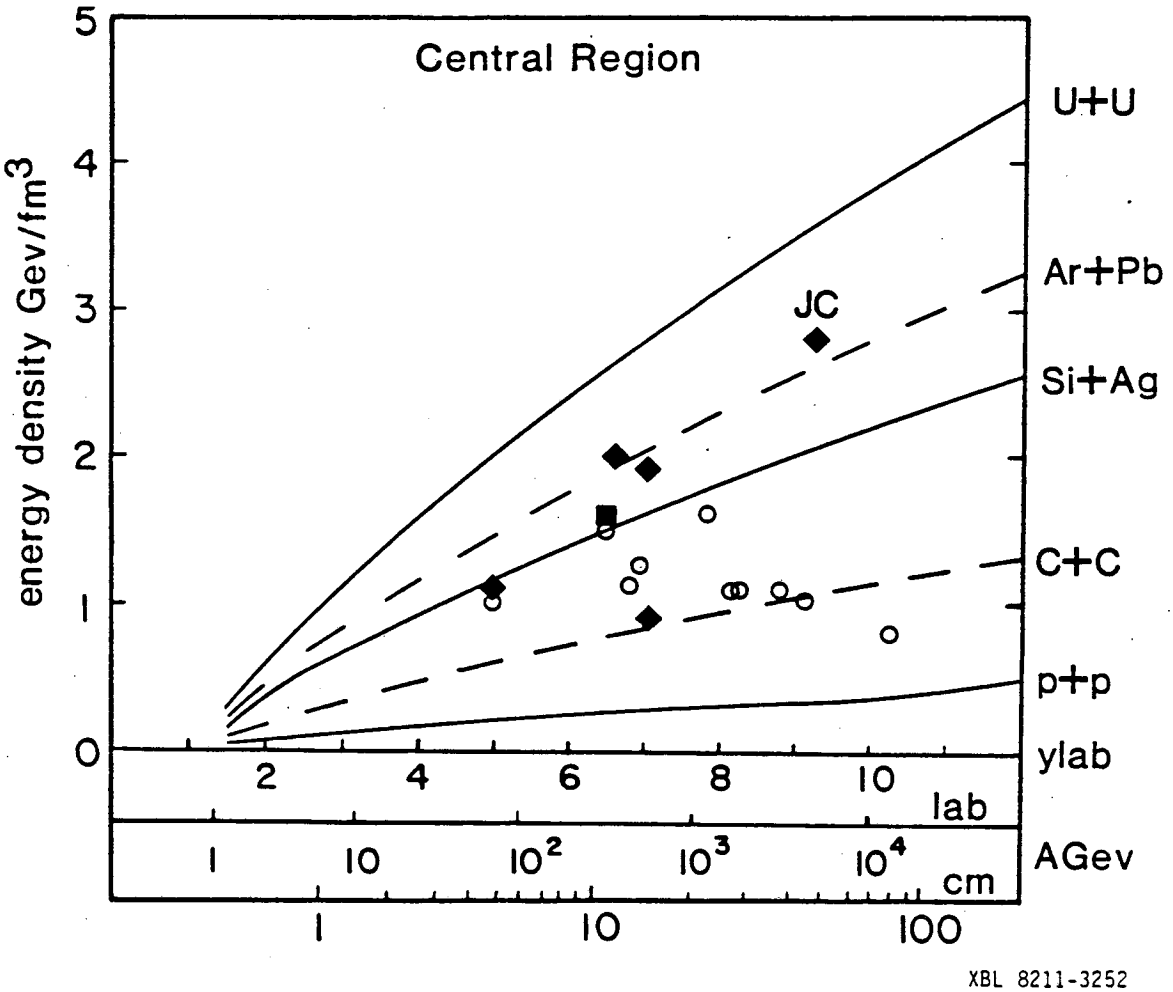
Central Region
energy density Gev/fm3
5
4
3
2
1
0
U+U
Ar+Pb
Si+Ag
C+C
p+p
JC
ylab
2
4
6
8
10
lab
AGev
1
10
10^2
10^3
10^4
cm
1
10
100
XBL 8211-3252

Fig. 18

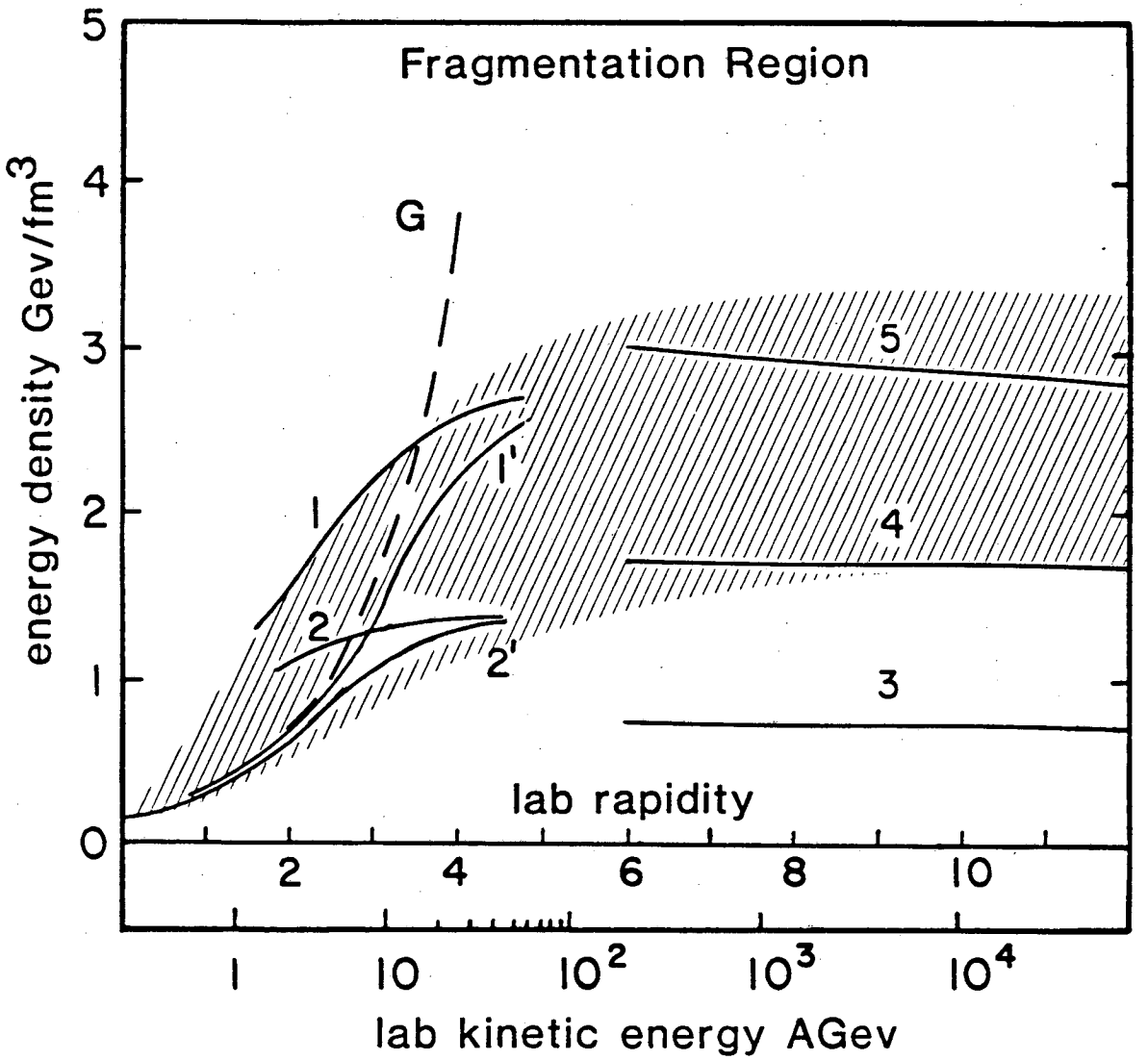

XBL 8211-3254

Fig 19

This report was done with support from the Department of Energy. Any conclusions or opinions expressed in this report represent solely those of the author(s) and not necessarily those of The Regents of the University of California, the Lawrence Berkeley Laboratory or the Department of Energy.

Reference to a company or product name does not imply approval or recommendation of the product by the University of California or the U.S. Department of Energy to the exclusion of others that may be suitable.

TECHNICAL INFORMATION DEPARTMENT
LAWRENCE BERKELEY LABORATORY
UNIVERSITY OF CALIFORNIA
BERKELEY, CALIFORNIA 94720